The loops facing the active site of prolyl oligopeptidase are crucial components in substrate gating and specificity

Zoltán Szeltner[a #], Tünde Juhász[a], Ilona Szamosi[a], Dean Rea[b], Vilmos Fülöp[b], Károly Módos[c], Luiz Juliano[d], and László Polgár[a]

[a]*From the Institute of Enzymology, Research Centre for Natural Sciences, Hungarian Academy of Sciences, H-1025 Budapest, Pusztaszeri út 59-67, Hungary,* [b]*Department of Biological Sciences, University of Warwick, Gibbet Hill Road Coventry CV4 7AL, UK,* [c]*Institute of Biophysics and Radiation Biology, Semmelweis University, Budapest, Hungary,* [d]*Departamento de Biofísica, Universidade Federal de Sao Paulo, Brazil.*

[#]Author, to whom correspondence should be addressed: Zoltán Szeltner, Institute of Enzymology, Research Centre for Natural Sciences, Hungarian Academy of Sciences, Budapest H-1518 P.O.Box 7. Tel: 36-1 279-3127; Fax: 36-1 466-5465; E-mail: szeltner@enzim.hu.

Abstract

Prolyl oligopeptidase (POP) has emerged as a drug target for neurological diseases. A flexible loop structure comprising loop A (res. 189-209) and loop B (res. 577-608) at the domain interface is implicated in substrate entry to the active site. Here we determined the kinetic and structural properties of POP with mutations in loop A, loop B and in two additional flexible loops. POP lacking loop A proved to be an inefficient enzyme as did POP with a mutation in loop B (T590C). Both constructs displayed an altered substrate preference profile. Ligand binding become markedly degraded. Conversely, the T202C mutation increased the flexibility of loop A, enhancing the catalytic efficiency beyond that of the native enzyme. The T590C mutation in loop B increased the preference for shorter peptides, indicating a role in substrate gating. Loop A and the His loop housing the catalytic histidine are disordered in the H680A mutant crystal structure, implying coordinated structural dynamics of these loops. A 17-mer peptide could not inhibit variants possessing malfunctioning loop A. This substrate may bind non-productively to an exosite involving loop A or to an open enzyme form. Biophysical studies suggest that mammalian POP resides in a predominantly closed conformational state, especially at physiological conditions. The flexible loop A, loop B and His loop system at the active site is the main regulator of substrate gating and specificity and represents a new inhibitor target.

Keywords: Prolyl oligopeptidase; Protein engineering; Enzyme catalysis; Differential scanning calorimetry; Enzyme structure; X-ray crystallography

Abbreviations: Abz, 2-aminobenzoyl; BNA, β-naphthylamide; CD, circular dichroism; DLS, dynamic light scattering; DSC, differential scanning calorimetry; DTT, dithiothreitol; DTNB, 5,5'-dithiobis(2- nitrobenzoic acid); EDTA, ethylenediaminetetraacetic acid; EDDnp, N-(2, 4-dinitrophenyl)-ethylenediamine; MES, 4-morpholineethanesulfonic acid; MD, molecular dynamics; Ni-NTA, nickel-nitrilotriacetic acid; GSH, reduced glutathione; GSSG, oxidized glutathione; PAGE, polyacrylamide gel electrophoresis; PBS, phosphate buffered saline; PCR, polymerase chain reaction; POP, prolyl oligopeptidase; Phe(NO_2), p-

nitrophenylalanine; res., residue; SEC, size-exclusion chromatography; TEV, tobacco etch virus; T_m, melting temperature

1. Introduction

Prolyl oligopeptidase (POP, PREP, PEP) (EC 3.4.21.26) is a member of a family of serine peptidases unrelated to the classic trypsin and subtilisin. The family includes enzymes of different specificities, like POP itself, dipeptidyl peptidase IV, acylaminoacyl peptidase, and oligopeptidase B [1]. POP is a cytosolic enzyme that selectively cleaves oligopeptides not greater than ~30 amino acids in length. POP is implicated in the metabolism of peptide hormones and neuropeptides [2-4] although some of the previously identified neuropeptide substrates do not appear to be hydrolyzed *in vivo* upon closer inspection [5]. Specific inhibitors have been shown to relieve scopolamine-induced amnesia [6], to ameliorate memory loss caused by age, brain lesions, or amnesic drugs [7, 8] and were neuroprotective under various conditions [9-11], resulting in significant pharmaceutical and academic interest. It was reported that POP has roles in the phosphoinositide cycle [12-14], intracellular transport [15], cellular differentiation [16], inflammation [17], angiogenesis [18], and cancer development [19]. Involvement in some processes may involve non-catalytic protein-protein interactions [4, 14]. POP is emerging as an important drug target in neurological diseases.

The crystal structure of POP [20] showed that the enzyme is composed of a catalytic domain with an α/β-hydrolase fold and a 7-bladed β-propeller domain. The β-propeller domain covers the active site situated in a central cavity at the domain interface and excludes large, structured peptides. Crystal structures of POP-ligand complexes show the ligand completely buried in the interior of the enzyme, and therefore do not reveal how substrates access the active site. Clearly, conformational changes are involved, as was demonstrated earlier when kinetic isotope effects showed that the rate-determining step of catalysis is a physical rather than a chemical step [21]. As the circular structure of the β-propeller stabilized only by hydrophobic interactions, it was suggested that substrates could be gated between the first and last propeller blades, allowing only short peptides into the active site via the propeller central tunnel [22]. However, the propeller domain of POP was found to be too rigid for such a regulatory function [23]. Limiting the flexibility between the propeller and catalytic domains with an engineered disulfide bridge inactivated the enzyme [24]. Flexibility of the loop structure at the domain interface was suggested to be required for efficient catalysis [24, 25]. This loop structure comprises a loop of the propeller domain (loop A, res. 189-209), a facing loop of the peptidase domain (loop B, res. 577-608), and other catalytically important loops as seen in Fig. 1. In contrast to former crystal structures of POP displaying the two domains in a closed position, the crystal structure of *Sphingomonas capsulata* POP revealed the enzyme in an open state, in which the peptidase and propeller domains are widely separated about a hinge region. This suggested that the substrate approaches the active site between the two domains [26]. The authors proposed that the enzyme resides in a closed resting state, and incoming peptide induces domain separation. Stabilization of the open state was explained by crystal packing constraints leading to the insertion of the polyhistidine tag of a neighboring molecule between the domains. Recently, another bacterial (*Aeromonas punctata*) POP structure was determined, showing the enzyme in the open state, this time without stabilization by crystal packing [27]. The inhibitor Z-pro-prolinal was soaked into these crystals, and due to the loose crystal packing, ligand binding and consequent domain closure could occur without crystal destruction, resulting in the closed state, ligand-bound crystal structure. The authors propose that POP resides in an open resting state, and substrate binding

causes domain closure in an induced fit mechanism. Despite the bacterial POP crystal structures, it is still unknown whether the enzyme in solution is in an open or closed resting state or in equilibrium between the two states. Crystal structures of ligand-free porcine POP in the closed state demonstrate that ligand binding is not required for domain closure, and that at least some of the enzyme molecules reside in the resting closed state. However, it is also possible that the enzyme remains closed during catalysis, requiring only movements of loop A and/or other loops and only limited inter-domain movements to allow substrate entry, as was suggested by earlier MD simulation studies [25] and by a recent study [28]. If this is the case, the open state observed in the bacterial crystal structures may be an artifact. Alternatively, eukaryotic POPs may differ from the bacterial enzymes in respect of their resting states.

In this work, we demonstrate that the flexible loop system involving loop A, loop B, and the loop holding the catalytic His (His loop) are important elements of the substrate gating mechanism and are required for the fine control of the catalysis. We also show that the conformational state of POP is very sensitive to, and dependent on, conditions in solution such as pH, ionic strength, and protein concentration. Our results suggest that mammalian POP resides in a predominantly closed but very flexible state under physiological conditions.

2. Materials and methods

2.1. Protein engineering and mutagenesis

The construction, expression, and purification of the variants mutated in loop A and loop B (T202C and T202C/T590C, respectively) and of the variant lacking loop A are described in [28]. Novel mutants (T204A, H680A and D149A) were created using complementary mutagenic primers, the wild-type POP bearing pSKPOP plasmid as template and the Quick Change Lightning PCR-based mutagenesis kit and protocol (Stratagene). The mutated proteins were expressed in a Rosetta *E. coli* strain and purified as described for the wild-type POP elsewhere [29].

2.2. Prolyl oligopeptidase activity assays

Routine activity assays were executed in a four-component buffer of 25 mM acetic acid, 25 mM glycine, 50 mM MES, 75 mM Tris, 1 mM EDTA, 1 mM DTT (standard buffer) and at 25 °C, which buffer system ensures constant ionic strength over a broad pH-range. The activity of prolyl oligopeptidase was measured with the following substrates: dipeptide Z-Gly-Pro*BNA, tetrapeptide Abz-Ser-Pro*Phe(NO_2)-Ala, heptapeptide Abz-Gly-Phe-Arg-Pro*Phe(NO_2)-Arg-Ala, octapeptide Abz-Gly-Phe-Gly-Pro*Phe-Gly-Phe(NO_2)-Ala, nonapeptide Abz-Glu-Gly-Phe-Gly-Pro*Phe-Gly-Phe(NO_2)-Ala and heptadecapeptide Abz-Gly-Phe-Ser-Pro*Phe-Arg-Ser-Ser-Arg-Ile-Gly-Glu-Ile-Lys-Glu-Glu-Gln-EDDnp prepared with solid phase synthesis (asterisks represent the cleavage sites). The reactions were measured fluorometrically at 25 °C using a Cary Eclipse fluorescence spectrophotometer (Varian Inc., Sydney Australia) equipped with a Peltier four-position multicell holder accessory and a temperature controller. The excitation wavelengths was 340 nm for the di-, 337 nm for the tetra-, hepta-, octa-, and nonapeptide, and 320 nm for the heptadecapeptide, while the emission wavelength was 420 nm for all substrates. The specificity rate constants (k_{cat}/K_m) were determined under first-order conditions; i.e. at substrate concentrations at least ten times lower than K_m. The first-order rate constant, calculated by nonlinear regression analysis, was divided by the total enzyme concentration to provide k_{cat}/K_m. Theoretical curves for the bell-shaped pH-rate profiles were calculated by nonlinear regression analysis, using the equation of $k_{cat}/K_m = k_{cat}/K_m(\text{limit})[1/(1 + 10^{pK_1 - pH} + 10^{pH - pK_2})]$ and the GraFit software (Leatherbarrow [30]). The k_{cat}/K_m (limit) stands for the pH-independent maximum

rate constant and K_1 and K_2 are the dissociation constants of the catalytically competent base and acid, respectively. When an additional pH-dependent effect modifies the bell-shaped character of the pH dependence curve, the data were fitted to equation of $k_{cat}/K_m = k_{cat}/K_m(\text{limit})_1[1/(1 + 10^{pK_1 - pH} + 10^{pH - pK_2})] + k_{cat}/K_m(\text{limit})_2[1/(1 + 10^{pK_2 - pH} + 10^{pH - pK_3})$ (doubly bell-shaped) curve. The limiting values stand for the pH independent maximum rate constants for the two active forms of the enzyme and K_1, K_2, K_3 are the apparent dissociation constants of the enzymatic groups, whose state of ionization controls the rate constants.

The K_i values, the dissociation constants of the enzyme-inhibitor complex, were measured in the standard buffer at pH 8.0. The inhibitor, KYP-2047 (4-phenylbutanoyl-l-prolyl-2(S)-cyanopyrrolidine) was synthesized by the University of Eastern Finland. The reaction mixtures were preincubated for 40 min at room temperature before the initial rate measurements. Data were fitted to the equation, $v_i/v_0 = 1/(1 + I/K_i)$, where v_i and v_0 are the initial rates in the presence and in the absence of the inhibitor determined at less then 5 % consumption of the substrate (Z-Gly-Pro-BNA).

The Michaelis-Menten parameters (k_{cat} and K_m) were determined with initial rate measurements (when K_m was sufficiently high), or with progress curve measurements (when the low K_m did not permit initial velocity measurements). The kinetic parameters were calculated with nonlinear regression analysis using the equation of $v = V_{max} * S / (K_m + S)$ or the integrated Michaelis-Menten equation [31].

The K_i of the substrate inhibition of the heptadecapeptide was determined by extrapolating the exponentially increasing (upon decreasing the substrate concentration) initial rates to zero substrate concentration (yielding the value of v_0) and fitting the points to the $v_i/v_0 = 1/(1 + S/K_i)$ equation, where v_i are the rates in the presence of various amount of substrate (S) and v_0 is the extrapolated rate in the absence of the inhibiting substrate.

Rate-limiting general acid/base catalyses were tested by measuring kinetic deuterium isotope effects at discrete pH values in 50 mM phosphate buffer containing water or heavy water (99.8%) and also containing 1 mM EDTA and 1 mM dithiotreitol. The deuterium oxide content of the reaction mixtures was at least 98%. The specificity rate constants (k_{cat}/K_m) were determined as in the case of the routine activity assay measurements. The pD of the deuterium oxide solutions was obtained from pH meter readings according to the relationship pD = pH (meter reading) + 0.4 [32].

2.3. Disulfide bridge formation in the T202C/T590C variant

The formation of the disulfide bridge between loop A and loop B (between the two cysteines introduced by site-specific mutagenesis) was executed as described in [28], using a GSSG/GSH redox buffer. An even lighter oxidation condition was applied preceding the DSC studies: the T202C/T590C variant was incubated at a GSSG concentration as low as 0.05 mM in a buffer of 20 mM phosphate, 0.5 mM EDTA, pH 8.0, for 18 hour.

2.4. Differential scanning calorimetry

The measurements were carried out with a Microcal VP-DSC (Microcal Inc.) in 20 mM sodium phosphate buffer (pH 8.0), containing 0.5 mM EDTA using a scan-rate of 60 °C/hour. The protein concentrations were about 4 µM. Samples with the inhibitor (KYP-2047, at 130-150 µM concentrations) were preincubated for 30 min at room temperature, degassed under vacuum and centrifuged for 30 min with 21,000g. The structural effects of the hepta- and heptadecapeptide substrates (3-26 µM) on POP were evaluated using a catalytically inactive variant (S554A). Step-heating experiments were also carried out by sequentially heating POP to a given temperature value, then cooling down to the starting temperature (25 °C) and again heating to an upper temperature value. The next steps were applied: 25-41.7 °C, 25-48.5 °C, 25-51.6 °C, and 25-55.4 °C. In a separate study wild-type

POP was heat treated in 200 µl PCR tubes in a water bath at 45 °C, 47.5 °C, 50 °C and 60°C in the DSC buffer for 10 minutes, then mixed with the loading buffer in 1:1 proportion and applied to native gels. Native PAGE was carried out with the method of Laemmli (1970).

2.5. Circular dichroism

Measurements were carried out with a Jasco J-720 CD spectropolarimeter in 10 mM phosphate buffer, pH 7.2, at 25 °C, using cells of 1.0 cm path length. Protein concentrations were about 1 mg/ml = 12.5 µM. Spectra were acquired at a scan speed of 10 nm/min in a wavelength range of 310-250 nm, averaging three scans. The spectra of the buffer were subtracted. The CD values were normalized to molar ellipticities.

2.6. Gel electrophoresis

SDS-PAGE was executed according to Laemmli (1970). Native gel electrophoresis was carried out the same way but SDS was omitted from the sample and running buffers. Wild-type POP (4.7 µM) and loop A^- POP (7.2 µM) were incubated with the irreversible inhibitor KYP-2047 in about 30-50-fold molar excess of KYP-2047 at 25°C for 30 min then applied to a native 10 % Laemmli gel. Controls without inhibitor were also preincubated at the same conditions. Native PAGE runs were also executed in a continuous format, without stacking gel or in discontinuous format with stacking and separation gels, but with separation and running buffers adjusted to a lower pH value (pH 7.9) in order to examine the contribution of concentration by the stacking gel and/or the pH to the generation of the POP forms with different mobilities. Wild-type POP was applied to the gels in decreasing concentrations (from 3.58 to 0.71 µM), when analyzed with Coomassie Blue R-250 staining or diluted up to the concentration of the native POP in the brain samples when detected with western blot. Human brain samples were extracted in 50 mM phosphate buffer, containing 100 mM NaCl, 5 mM EDTA, 5 mM DTT, 1 µM pepstatin A, 2 µM bestatin, 50 µM leupeptin, 1 mM benzamidine, using a mini bead beater (Glenmills) and zirconium-oxide grinding media (2x 1.5 min shaking at maximal frequency on ice). After centrifugation at 21,000 g at 4 °C and for 30 min, the extracts were aspirated and applied to 10 % native gels in a 1:1 dilution with the loading buffer.

2.7. Dynamic light scattering

The size distributions of POP (1 mg/ml) in 50 mM phosphate buffer, containing 1 mM EDTA, 1 mM DTT, either no NaCl or 300 mM NaCl (pH 6.5 or 8.0), or in 1x PBS buffer (pH 7.4) were assessed by an ALV goniometer at 25 and at 37 °C with a Melles Griot diode-pumped solid state laser at 457.5 nm wavelength (type: 58 BLD 301). The intensity of the scattered light was measured at 90° at room temperature. The autocorrelation function was calculated using an IBM PC-based data acquisition system developed in the Institute of Biophysics and Radiation Biology, Semmelweis University. The most probable particle distribution was estimated using the maximum entropy method that produces normalized distribution [33]. The hydrodynamic radii of the particles were calculated based on the Einstein-Stokes equation. The polydispersity index (PI, the relative variance) of the peaks was calculated. If this index were higher than about 0.04, we tried to separate the peaks into Gaussian components. POP was buffer exchanged and re-purified by SEC on a Superpose 12 column, concentrated to 1 mg/ml and kept at 4 °C prior to the measurements.

2.8. Crystallization, X-ray data collection and structure refinement

The H680A variant was crystallized using the conditions established for the wild-type enzyme except the pH of the buffer was between 6.5 and 7.5. X-ray data were collected on the IO4 beamline at the Diamond synchrotron (UK) using an ADSC Q315r CCD detector.

All data were indexed, integrated and scaled using the XDS package [34]. Subsequent data handling was carried out using the CCP4 software package [35]. Crystals belong to the orthorhombic space group $P2_12_12_1$, there is one molecule in the asymmetric unit, with the solvent content of 48% by volume. Refinement of the structure was carried out by alternate cycles of REFMAC [36] and manual refitting using O [37]. Water molecules were added to the atomic model automatically using ARP [38] at the positions of large positive peaks in the difference electron density, only at places where the resulting water molecule fell into an appropriate hydrogen bonding environment. Restrained isotropic temperature factor refinements were carried out for each individual atom. Data collection and refinement statistics are given in Table 5. The coordinates and structure factors have been deposited in the RCSB Protein Data Bank as XXXX.

3. Results

3.1. Engineering POP

Fig. 1A shows the overall structure of the POP molecule while Fig. 1 B highlights the modified part. The flexible loop structure involving loop A and loop B, and other catalytically important loops is displayed. Mutations were introduced into loop A (T202C, T204A), loop B (T590C), His loop (H680A) and into loop D (D149A). A further construct, lacking loop A was also created. As Fig. 2 shows, even the extreme intervention of loop A removal did not perturb the tertiary structure of POP appreciably, demonstrated by near-UV CD (Fig. 2A). The other variants (T204A, T202C, T202C-T590C and H680A) displayed identical far and near-UV CD spectra with the wild-type POP (not shown). DSC studies have also shown comparable thermal denaturation curves for the loop A and B variants of which two (scans for the wild-type and the loop A^- POP) are shown in Fig. 2B. Only slight reduction in the thermal stability can be observed for the loop A^- enzyme.

3.2. Most of the mutations in the flexible loop structure change the catalytic power, the pH and salt dependencies of substrate hydrolysis and the rate-determining step of the catalysis

Fig. 3 shows the pH dependences of the specificity rate constant (k_{cat}/K_m) for the loop A and B variants using the short substrate Z-Gly-Pro-BNA. The inserts in Fig. A, B and D show the pH-dependent kinetic isotope deuterium effects. As presented in Fig. 3 and detailed in Table 1, the pH dependences and the limiting values of k_{cat}/K_m changed within orders of magnitudes with the variants, except T204A.

Wild-type POP displays a pH optimum of about 8.0 and a double bell-shaped pH-rate profile with a second maximum at the acidic side. Changing T204 to alanine did not change the pH-dependence and the activity significantly. In addition, both wild-type and T204A show no significant kinetic deuterium isotope effects in the physiological pH-range, indicating that the rate-determining step of the catalysis is a physical step. However, a significant isotope effect appears in the acidic pH-range, where POP is most flexible [39].

The T202C and the T202C/T590C variants (Fig. 3BC) show significantly changed pH-optima of about pH 7.0. Interestingly, the T202C variant displays about 2-fold higher enzyme activity than the wild-type POP if compared at their pH-optima. Moreover, the increase in rate is even more pronounced in the presence of 0.3 M NaCl (Fig. 3B). In this respect T202C POP behaves like the trypsin-nicked enzyme (published in [28]) where loop A was cleaved at its middle between D196 and S197. More interestingly, T202C variant displays a maximal kinetic deuterium isotope effect at its pH optimum (insert in Fig. 2B) suggesting that this mutation evokes a flexibility change in POP, or in a part of the molecule (in the mutated loop

A) similarly to the effect of the acidic pH in the wild-type enzyme. Partial digestion of this variant with trypsin as executed in [28], suggest that loop A is more accessible to trypsin compared with thee wild-type POP because trypsin can cleave loop A more easily (not shown).

When T590C mutation is introduced into loop B in addition to the T202C mutation in loop A, it rendered the enzyme very inefficient, with more than an order lower activity (Fig. 3C).

Almost negligible activity is observed with the variant lacking loop A (Fig. 3D). Its pH-rate profile is rather asymmetric and significantly broadens at higher ionic strength (300 mM NaCl) (Fig. 3E). Most importantly, this variant shows no kinetic deuterium isotope effect in the entire pH-range studied (insert in Fig. 3A).

Changing D149 that resides in a different propeller loop to alanine generated a variant with catalytic activity similar to that of the double mutant, but with an even lower pH optimum (Fig. 3C).

3.3. A chemical cross-link between loop A and loop B inactivates POP in a substrate size-dependent way

Previously, we have tested the effect of disulfide bridge formation on the activity of the double mutant T202C/T590C. Oxidation achieved by air oxygen or a glutathione redox buffer resulted in activity decrease of the variant measured with the short Z-Gly-Pro-BNA [28]. Extending the examination on the longer octapeptide and the especially long heptadecapeptide substrates, a complete inactivation was observed only for the long substrates while POP retained ~15 % of its original activity toward the short Z-Gly-Pro-BNA. Interestingly, the substrate-size preference of the variant was found to be also different from the wild-type even when C202 and C590 were in a reduced state in the presence of DTT. The ratio of specificity rate constants for the Z-Gly-Pro-BNA and the octapeptide hydrolysis was between 1.30-1.83 for the wild-type POP at low ionic strength and at pH 8.0, while this value was about 6-7 with the variant. The further change in the preference for Z-Gly-Pro-BNA over the longer octapeptide upon air and glutathione oxidation is presented in Table 2. The oxidized glutathione partially inactivated (30%) the wild-type POP too, but equally for both the shorter and the longer peptide, while the C255S control variant not containing the C255 responsible for the thiol-sensitivity of POP activity [40] retained the initial activity. 89 % and 87% of the activity of the glutathione-oxidized and air-oxidized T202C/T590C variant could be recovered with a DTT treatment (10 mM), respectively.

3.4. Mutations in the flexible loop structure change the substrate specificity

Four additional substrates with different sizes and amino acid compositions were also evaluated comparatively. A nonapeptide similar in amino acid composition to the octapeptide (a standard fluorescent peptide substrate widely used in our former studies), a heptapeptide similar in size but different in composition to the octapeptide, a tetrapeptide similar in size to Z-Gly-Pro-BNA but different in composition, and a large heptadecapeptide with a molecular mass of 2.61 kDa close to the 3 ~kDa cut-off limit for POP, were used. The amino acid composition of the substrates is found in the Materials and methods section. The substrate hydrolysis profiles, i.e., the variation of the specificity rate constants with the different substrates, were determined at the pH optima of the loop A and loop B variants at low and high ionic strengths and compared to the wild- type (Fig. 4). The profiles of the loop A^- and T202C variants are also displayed at pH 8.0 (Fig. 4A' and 4D').

Fig. 4A and A' present the substrate hydrolysis profile of the loop A^- variant. The most striking difference compared with the wild-type (Fig. 4C) is the poor hydrolysis of the relatively bulky and mainly uncharged substrates (the nonapeptide and the octapeptide),

while the small Z-Gly-Pro-BNA and the large and charged heptadeca substrates are relatively well hydrolyzed by the variant. The heptapeptide, containing two arginines at P2 and P2' sites, is by far the best substrate for the loop A^- enzyme (Fig. 4A), which was not the case for the wild-type POP that hydrolyzes all substrates of interest with comparable rates (Fig. 4C). The sensitivity to ionic strength was also modified by the mutations. Loop A^-, T202C/T590C and T202C variants show unchanged or slightly decreased activity with the octa-, and nonapeptide substrates at higher ionic strength, while wild-type POP displays positive salt effects.

3.5. Mutations in the flexible loop structure have dramatic effects on substrate and inhibitor binding

As shown above, removing the entire loop A rendered POP catalytically very inefficient, with a specificity rate constant (k_{cat}/K_m) of 200 $M^{-1}s^{-1}$ compared to the 4.4×10^6 $M^{-1}s^{-1}$ for the wild-type enzyme at pH 8.0 and at low ionic strength (Table 3). The 20,000-fold impairment could mainly be attributed to a very weak binding of the substrates to the variant. The low water solubility of Z-Gly-Pro-BNA did not permit the determination of the kinetic parameters (k_{cat} and K_m) but using the highly soluble heptapeptide (Table 3), we observed a 200-fold increase in K_m and a 13-fold reduction in k_{cat} upon removing loop A. In contrast, only an 11.5-fold increase in K_m and a slightly increased k_{cat} was found for the T202C/T590C variant. Binding of the octapeptide to the almost inactive loop A^- enzyme was undetectable in a titration experiment performed as in [24] (data not shown). Inhibitor binding is also drastically reduced. The K_i with the highly potent irreversible inhibitor KYP-2047 increased from 0.13 nM (for the wild-type enzyme) to 1.0 µM for the loop A^- variant (Table 3 and Fig. 5AB).

3.6. Inhibition with the heptadecapeptide is missing when loop A is removed

As marked with an asterisk on Fig. 4C, D, and D', the large heptadecapeptide displays a striking substrate inhibition, which prevented determination of the kinetic parameters with this substrate. Fig. 6A and B show the increasing k_{cat}/K_m or initial rate of the reactions, respectively, upon reduction of the substrate concentration. The rate increased exponentially even when the sensitivity limit of the instrument was reached. Extrapolating to the zero substrate concentration, the specificity rate constant with this substrate would reach a value (limit = 4.13×10^6) close to that with Z-Gly-Pro-BNA. The approximate inhibition constant (K_i) for the heptadecapeptide is about 0.25 µM (Fig. 6B). Removing loop A completely abolished the substrate inhibition, and the efficiency of hydrolysis of this very large substrate approaches that of the shorter Z-Gly-Pro-BNA. Interestingly, the inhibition was also absent in the case of the T202C/T590C variant, suggesting the involvement of loop B too in the process (Fig. 4B).

3.7. The differences in the ligand-binding capacities can also be detected in structural assays

The presence of the inhibitor (KYP-2047) in high molar excess had no observable effect on the running profile of the loop A lacking enzyme in native PAGE, as seen in the insert of Fig. 5B. In contrast, KYP-2047 (and PP211, in an earlier study [41]) caused significant alteration in the relative amount of the different POP forms (marked with 1, 2, 3) as well as in the mobility of the lowest form in particular, in the case of the wild-type enzyme (Fig. 5A). The T204A variant, displaying wild-type properties, behaved the same way (not shown).

The inhibitor-bound wild-type POP displays enhanced thermostability when investigated with DSC. The thermal denaturation profile of the POP-inhibitor complex simplifies from a

double peak character with two melting temperatures to a single melting point, with an elevated T_m value (Fig. 7A). Similar results were obtained with the T204A and the T202C variant (not shown). However, the DSC profiles of the loop A^- POP and the double mutant (T202C/T590C) showed a decreased stabilization effect (Fig. 7B), indicating weaker inhibitor binding. The T_m of the first transition increased significantly, while the second transition remained nearly unchanged, therefore, the two peaks fully (T202C/T590C) or partially (loop A^-) merged. The concentration of the inhibitor in the samples was high enough to saturate both variants, since only about 1%, remaining activity could be measured prior to DSC scans. However, both variants regained their original activity upon high dilution suggesting that inhibition is reversible and not covalent as observed with the wild-type enzyme.

The impact of the formation of the interloop disulfide bridge between C202 and C590 on the structure and inhibitor binding could also be detected with DSC. The first transition did not develop and protein melted with a single broad transition that was hardly influenced by the presence of KYP-2047 (Fig. 7D).

The binding of the inhibiting heptadecapeptide to an inactive POP variant (S554A) was again detected with DSC. The first transition was influenced (Fig. 6C and D). It is worthy of note that the heptapeptide (Abz-Gly-Phe-Arg-Pro-Phe(NO_2)-Arg-Ala) that was found to be the best substrate for POP (K_m is about 0.4 µM) elicited only subtle change in the DSC profile while the heptadecapeptide completely abolished the appearance of the first transition at the same concentration (26 µM) (Fig. 6 CD). Despite this, when inactive S554A POP was co-crystallized with the heptadecapeptide, no electron density was visible for the peptide. This suggested two possibilities for the interaction, binding in multiple sites simultaneously and weakly or binding to the open state of POP, whilst only the closed state is crystallized. In order to test the possibility of POP in an open form, we performed further structural assays.

3.8. The transition peak with lower T_m in DSC may indicate a heat-induced conformational change

As shown above POP is melting in two transitions during a DSC run. Interestingly, a large polyhistidine tag (21 a.a.) in the N-terminus of the protein can change the thermal denaturation curve significantly (dotted line on Fig. 7A). The first transition becomes more pronounced and appears with a lower T_m, while the second one develops at higher temperature, compared to the native POP. Similar peak separation can be observed with the loop A^- variant (Fig. 2B). When POP is heated over the T_m of the first transition (Line 3 in Fig. 7C) and cooled down then reheated, this transition does not appear again, indicating an irreversible structural change. After this transition point is reached, the structure is stabilized, reflected in a gradual increase in the starting temperature of the second transition, as shown in Fig. 7C (lines 4 and 5). An aggregation process is seen when analyzing the heat-treated (up to 60 °C) samples with native PAGE (insert of Fig. 7C). The first transition never appears if loop A and loop B is joined by a disulfide bridge (Fig. 7D black curve). An even earlier and very broad first transition (black curve in Fig. 7A) is observed with a mutant (D149A), where the salt bridge (D149A-R643) and the double hydrogen bonds (white dotted lines in Fig. 1B) between the propeller (white loop in Fig. 1B) and the peptidase domain cannot form. These results suggest that the first transition represents an opening of a closed enzyme structure.

3.9. The closed state of POP appears to be predominant at physiological conditions

Native PAGE revealed three forms of POP with different mobilities (Fig. 8). However, these forms appear to be generated by the highly concentrating action of the stacking gel as when samples are run on continuous gels without stacking (Fig. 8B) only the highest-mobility and likely the most compact form is present. Varying the pH of the running buffer

and the separating gel, no alteration in the running profile could be seen. Interestingly, only the most compact POP form could be detected when applying human brain lysate to gels either with or without a stacking portion (Fig. 8C).

3.9. Dynamic light scattering suggest conformational heterogeneity of POP that is highly influenced by pH and ionic strength

Seeking for signs of heterogeneity, e.g. more POP forms in solution, we utilized DLS (Fig. 9), a technique suitable for characterizing size distribution of proteins in solution not influenced by matrix effects unlike native PAGE or SEC. The hydrodynamic radii (R_h) obtained in various conditions (Table 4) demonstrate that in most cases POP indeed displays heterogeneity in size. The highest uniformity was observed at low ionic strength, at pH 6.5, where POP possesses a hydrodynamic radius of 3.44 nm. A similar state can be observed at pH 8.0, at higher ionic strength, with a slightly higher R_h value of 3.60 nm. At all other conditions, we obtained broader curves assuming two differently sized forms at various proportions (Table 4). Preincubating POP with the inhibitor KYP-2047 at pH 8.0, 300 mM NaCl, converted the material with an R_h of 3.77 nm to a more compact one with an R_h of 3.24 nm. Similar but not perfect conversion could be observed at pH 6.5 in the absence of salt. Interestingly, no such a conversion by KYP-2047 could be detected at 37 °C. It is also shown in Table 4 that various mutants of POP are also characterized by a broad size-distribution containing populations of larger and smaller molecules.

3.10. Crystal structure of the H680A variant reveals cooperation between loop A and the catalytic His loop

In order to probe the role of the loop containing His680, the H680A mutant was crystallized and the structure was determined. This mutant crystallized in the closed conformation. In the closed-state wild-type enzyme His680 lies between, and is hydrogen bonded to, the catalytic Ser554 and Asp641, completing the catalytic triad (Fig. 10). Loss of these interactions in the H680A mutant renders the His loop (residues 677-681) more flexible and a different conformation is adopted (Fig. 10). The loop is traceable but has weak electron density and the average B-factor is significantly higher at 40 $Å^2$ compared to 17 $Å^2$ for the rest of the structure. This local loop reorganization breaks a hydrogen bond between the main chain carbonyl of His640 and the main chain amide of Ala678. This increases the mobility of His640 and allows this residue to swing out towards the surface of the protein where it clashes with loop A (residues 192-201), forcing this loop to adopt a different conformation that explains why it is disordered in the H680A structure. This mechanism suggests cooperativity of the structural dynamics of the His loop and loop A.

4. Discussion

4.1. The flexible surface loop structure of POP fine-tunes potential inter-domain fluctuations during catalysis.

Despite extensive research and a wealth of accumulated knowledge on the action of POP, it is still not clear how substrates access the buried active site of the enzyme. Crystal structures of bacterial POP in an open state and substrate-induced domain closure upon ligand binding [26, 27] suggest substrate entry between the peptidase and propeller domains that separate in a hinge-like manner. It is not yet apparent if the mammalian enzyme structure can open up as does the bacterial enzyme in the crystal structures. All existing crystal structures of mammalian POP show a closed state, even in the absence of ligands.

Recent computer simulation studies suggest a mechanism whereby substrates enter the active site through a loose surface loop structure that does not involve domain separation [25], [28]. The motion and rearrangement of the flexible loop structure involving loop A and the facing loop B are postulated to regulate substrate and inhibitor entry and binding to the active site. Loop A was predicted to be the main protagonist in this substrate gating by adopting open and closed positions. Inhibitor binding stabilized the closed state in the simulation runs. This was experimentally supported by a trypsin cleavage assay where trypsin was unable to cleave loop A when inhibitor (KYP-2047) was bound to POP.

Loop A (T202C) and loop B mutants (T590C) and a loop A deficient POP were generated. It was shown that joining loop A and loop B in a double mutant (T202C/T590C) with a disulfide bridge between the two introduced cysteines abolished the enzyme activity, indicating that the free movement of loop A is required for the catalysis and might be responsible for the gating. The catalytic power of the loop A and loop B point mutants changed significantly, even if the introduced cysteines were in reduced form in the presence of DTT [28].

In order to elucidate the underlining mechanisms, further enzyme kinetic and structural studies involving pH dependence, ligand binding, CD, DSC, PAGE and DLS assays were performed with the variants. The changes in the substrate specificities and substrate size preferences were also investigated. We have also attempted to find experimental evidence for the presence of different POP forms in our porcine POP preparations and human brain samples.

Since molecular dynamics studies suggested an important role for T204 of loop A in the loop A/loop B interaction via an H-bond network [28], this amino acid was mutated to alanine. Two additional mutants were also created. In the open state crystal structures of the bacterial POP enzymes [26] both loop A and the loop containing the catalytic triad histidine (His loop) are disordered. Therefore, we changed H680 to alanine in an attempt to destabilize the closed form of mammalian POP. The D149A mutant was also engineered for a similar purpose since this mutation abolishes the formation of the double H-bonds (white dotted lines on Fig. 1B) between D149 and R643 that stabilize the closed state.

As we have demonstrated (Fig. 3 and Table1) mutations in the flexible loop structure markedly changed the catalytic power of POP resulting in orders of magnitude differences in activity. The pH-optimum of POP was also changed considerably, suggesting that mutations alter the catalytically relevant electrostatic interactions at the active site, which can markedly affect the binding and the route of the substrates to active site of POP [42]. A finely regulated functioning of the loop structure seems to be required for the mildly alkaline pH optimum of POP, at least with the neutral substrates like the short Z-Gly-Pro-BNA and the octapeptide. Whilst the variant lacking the entire loop A is by far the weakest catalyst, even more subtle modifications in loop A (T202C) and in the facing loop B (T590C) altered the catalytic behavior of the enzyme profoundly, illustrating the important role of this part of the structure. We note that mutation did not interfere with the overall structure of POP as was demonstrated with CD and DSC assays.

An almost complete loss of activity was observed when loop A and loop B was cross-linked with a disulfide bridge. However, complete inactivation was only seen for the bulkier octapeptide and heptadecapeptide. The formation of the chemical cross-link between loop A and loop B thus interferes with the substrate and inhibitor entry to the active site. Domain flexibility is also affected as reflected in the DSC scan (Fig. 7D). The relatively smaller effect on the entry of shorter substrate is consistent with either substrate entry mechanism; larger domain separation or more subtle loop separation only. If larger domain separation movements are involved, these must occur very fast given the high processivity of POP (k_{cat}/K_m ~ 5,000 mM^{-1} s^{-1}, and a k_{cat} of ~40 s^{-1} with Z-Gly-Pro-BNA [43]). This is evidently

limited by a need for conformational adaptation, as kinetic deuterium isotope studies suggested [21]. Considering the fact that only one semiconservative mutation in loop B (T590C) can also change the substrate-size preference toward the short Z-Gly-Pro-BNA substrate by a factor of about 4-5 (Table 2), the flexible loop system takes great part in the control of substrate gating. Moreover, the flexibility of loop A proved to be the main determinant in controlling the rate-determining step of the enzyme catalysis.

Mutations in the flexible loops altered not only the catalytic power, inhibitor-binding capacity of POP and the rate-determining step of the catalysis, but also the substrate specificity. The double mutant (T202C/T590C) (Fig. 4B) behaves very similarly to the loop A^- variant (Fig. 4A), sharing a comparable substrate hydrolysis profile. However, all variants described here are catalytically impaired when compared to native POP for hydrolysis of the relatively bulky and mainly uncharged octa- and nonapeptide substrates (Fig. 4C).

The proper functioning of loop A and loop B is evidently dependent upon stabilizing interactions that can be perturbed by even the semiconservative T/C mutations. In crystal structures of POP these loops adopt a well-defined structure that is stabilized by interactions (Fig. 1B) between the loops themselves (H-bond between T202 and T590) and between loop A and the N-terminal part of the protein (the K196-D35 salt bridge).

Two transiently formed H-bonds between T204 on loop A and K588 and H593 in loop B (Fig. 1B) was predicted by MD simulations, but only when inhibitors are bound to the active site [28]. Changing T204 to alanine did not result in significant alterations in the kinetic behavior of the enzyme (Fig. 3A). Inhibitor binding also did not change significantly (not shown), indicating that these potential H-bonds either are not essential or the main chain H-bond (A204-K588) still can form and is enough for the stabilization of loop A.

However, the strength of the T202-T590 H-bond (present in the crystal structures) and the K196-D35 salt-bridge could be significantly changed, modified in the point mutants and obliterated in the loop A^- variant as reflected in the change of the ionic strength sensitivity of the enzyme reactions (Fig. 4A). The relative efficiencies in the hydrolysis of smaller substrates are least perturbed, consistent with an earlier observation, where the elimination of the K196-D35 salt bridge resulted in a relaxed preference for shorter substrates [44]. An increased preference for shorter substrates was observed here for the loop B mutant (T590C), suggesting that both the K196-D35 salt bridge between loop A and the N-terminus and the interaction with loop B contribute to the stabilization of loop A and involve in the size-dependent gating.

Conversely, mutations weakening the interactions holding loop A in place enhanced catalysis, as was similarly observed in the trypsin-nicked enzyme that is cleaved in this loop [45]. This likely increases its opening frequency by shifting the equilibrium toward its open state. The highest catalytic efficiency was observed with the T202C variant, where T/C mutation may reduce loop stabilization, increasing loop flexibility by weakening interloop H-bond or decreasing the polarity of the loop microenvironment. Only this variant shows a significant kinetic deuterium isotope effect at neutral pH (insert in Fig. 3B), suggesting that flexibility is increased to the extent that conformational changes are no longer rate-limiting, unlike native POP. Trypsin digestion studies also support the increased flexibility and accessibility of loop A in T202C variant compared to the wild-type. The removal of the bulky loop A did not result in the appearance of a kinetic deuterium effect (insert in Fig. 3D), although this truncation could theoretically ease the passage of substrates to the active site by removing a steric barrier. These results suggest the active participation of loop A in substrate entry, the function of which is missing if loop A is removed.

The variants with altered loop A/B capabilities (loop A^- and T202C/T590C) also displayed no substrate inhibition with the heptadecapeptide, while the wild-type enzyme shows marked effect. This suggests that this large substrate binds to an external binding site

(possibly non-productively) that involves the contributions of loop A and/or loops B, and interferes with the gating. Other investigators, observing the inhibition of substance P hydrolysis by the bound calcitonin gene-related peptide [44] also proposed the presence of an unidentified exosite in POP. Whilst strong non-productive binding is consistent with the activity measurements (Fig. 6A and 6B) and DSC (Fig. 6C and 6D), no heptadecapeptide was observed in the electron density of the crystal structure of the inactive S554A variant crystallized in the presence of large quantities of this substrate. This could be because non-specific binding occurs in multiple sites simultaneously and weakly, and so was not captured crystallographically. Alternatively, this may be because the long heptadecapeptide binds to the open state, whilst only the closed state was crystallized.

The interaction with the large substrate interfered with the first transition in DSC that transition possibly represents domain separation. This transition is absent when loop A and loop B are crosslinked in the T202C/T590C variant, and this variant would likely prevent both loop opening and domain separation. However, this transition is also present in the thermal denaturation of the loop A^- variant (Fig. 2B), indicating that this thermally induced conformational change involves more than a simple opening of loop A. As seen in Fig. 7A, the large polyhistidine tag on the N-terminus (res. 1-75) markedly influences this earlier transition. The separation of this peak also present when loop A was clipped with trypsin or when the ionic strength was increased. This complex transition is therefore likely associated with movement of the N-terminal part of the molecule, but also movement of loop A and possibly domain separation. Weak inhibitor binding in the case of the loop A^- and T202C/T590C variants influenced the same transition, indicating that even weak inhibitor binding significantly stabilizes the structure against this conformational change. These results suggest that there is a fine-tuned coordination exists between the flexible loop system and the N-terminal part of the protein proving the validity of an earlier MD simulation study [25].

The need for the coordinated action of loop A and loop B is also evident from the kinetic results, as both removal of loop A and mutation in loop B generated enzymes with low catalytic activity and similar substrate preference. Thus, loop B mutations may act indirectly by disrupting normal loop A function. His680 is positioned between Asp641 and Ser554 to complete the catalytic triad. In previously determined crystal structures of S554A and D641N/D641A mammalian POP catalytic triad variants, His680 remains in the catalytically active position, with a fully ordered His loop and loop A visible in the electron density [43]. We engineered the H680A mutant to destabilize the active site network in the hope of shifting the equilibrium towards the open form. Despite this, the H680A structure determined in this work is once more in the closed state, but some significant structural differences give insight on the possible role of the loop structure. Overall, the mutated His loop becomes much less ordered, and loop A is completely disordered (Fig. 10). This can be understood by looking in detail at the structural changes resulting from the mutation. Firstly, the H680A mutation obviously results in the loss of the hydrogen bonds between H680 and the catalytic Ser554 and Asp641. In the absence of these interactions the His loop (residues 677-681) becomes much more flexible and adopts a different conformation from that found in the closed structure of native POP and other variants (Fig. 10). The His loop is traceable but has only very weak electron density, reflected by the average B-factor 40 $Å^2$, compared to 17 $Å^2$ for the rest of the structure. Further, the carbonyl of His640 lying adjacent to the mutated residue looses the usual H-bond with the main chain NH of Ala678. This renders His640 more mobile, causing this residue to swings out towards the surface of the protein. This increased mobility of the His loop is transmitted to loop A (residues 192-201), destabilizing this region entirely so that it is disordered in the structure. Significantly, the His loop and loop A are also disordered in the open state bacterial POP structures determined to date. This indicates a close coordination and potential cooperativity between the structural dynamics of

these loops during substrate gating and catalysis. The interplay between these two loops may be mediated by loop B and the Asp loop (Fig. 1B) since these evidently interact. The loop A^- variant exhibits an altered pH dependency and decimated substrate/inhibitor binding leading to the near abolishment of activity. In contrast, the loop A (T202C) and loop B (T590C) point mutants displayed altered ligand binding but relatively unaltered catalytic activity. Different again, in previous studies the Asp loop (D641A) and the Cys loop (C255A) variants showed altered pH dependencies, but ligand binding was only slightly affected [40, 43]. This implies a much greater corruption of the active site structure in the loop A^- variant. The H680A crystal structure helps to explain this, suggesting that removal of loop A would likely destabilize the His loop, and disrupting the catalytic triad. Unfortunately, the loop A^- and point mutants other than the H680A variant failed to yield crystals suitable for diffraction studies, precluding a more detailed structure-function correlation of these variants at present.

4.2. The resting state of mammalian POPs is likely a closed but very flexible conformational state

The three POP forms in native gels that included the highly concentrating stacking gels, were not present in gels lacking this stacking component (Fig. 8A). The forms were suggested to represent a closed (band 1) and an open enzyme (band 2) by other investigator [46]. Recent crystal structures of an archaea AAP, a related POP family enzyme, contain molecules in open and closed states in the crystal, in some cases even in the same dimer. This is suggestive of an equilibrium in solution comprising populations of open and closed forms, although crystal contact influences causing and/or stabilizing the open form can not be ruled out entirely. The authors suggest that eukaryotic and the bacterial enzymes can display differences in the resting states, due to the differences in the amino acid composition at the domain interfaces [47]. Supporting this mammalian POPs always crystallize in closed conformation even in the absence of ligands. Recent NMR studies on mammalian POP still suggest that POP possess both open and closed states in equilibrium at the relatively high protein concentration applied in NMR studies [48]. The observed potential shift in equilibrium towards the open form under conditions of high protein concentration may explain the additional bands (e.g. band 2) in native PAGE including the highly concentrating stacking gel (Fig. 8A). Intriguingly, endogenous POP from brain lysate did not exhibit additional forms in native PAGE (Fig. 8B and 8C), and neither did recombinant POP after incubation in the brain lysate (data not shown). This suggests that the equilibrium can be shifted toward the closed enzyme form at natural conditions by host factors, similarly to the artificial inhibitors. The possibility of endogenous cellular POP inhibitors has been suggested previously [49, 50].

In a different interpretation, POP forms in the native gels would be oligomers. We observed three main cross-linked POP bands on SDS gels, when POP was treated with glutaraldehyde [41], indicating that POP molecules are prone to form intermolecular interactions and may dimerise and tetramerise at higher protein concentration, although this might seem physiologically irrelevant. Some dimerisation is really observed when concentrated (> 8-10 mg/ml) POP is purified by SEC.

The DSC experiments suggest that POP is mostly closed at concentration of at about 4.0 µM. In this case DSC plots are interpreted as POP gradually adopting a more open state as the temperature increases, and finally opens fully at a certain temperature (T_m of transition one). The fully opened state may expose a large hydrophobic surface area, leading to irreversible aggregation (Fig. 7 C). This is supported by the lack of the first transition on strong inhibitor binding, where only the second transition (representing a complete denaturation) was observed. Such a strong stabilization (Fig. 7) was only seen with the wild-type POP, which also shows strong and irreversible inhibition. Those loop mutants

displaying only weak and reversible inhibitor binding still shows the first DSC transition (but with an elevated T_m) as well as the H680A mutant that really crystallized in a closed state. In the case of D149A variant, a very broad first transition was observed in DSC (Fig. 7A). This mutation removes a key inter-domain stabilizing interaction (D149-R643) that is conserved amongst the POP, oligopeptidase B, and acylaminoacyl peptidase subfamilies of the POP family [51]. The broad first transition in the DSC could correspond to a less cooperative, but even a closed structure. The broadest curve was observed for D149A variant in DLS suggesting a more flexible structure or alternatively a shift in the equilibrium toward the open state, with a higher R_h value. Unexpectedly, conversion into a high R_h form upon temperature increase (from 25 °C to 37 °C) observed for the wild-type POP, no such change was detected for the D149A variant (Table 4). This behavior is more consistent with a model, where DLS shows only change in flexibility and not distinct (closed and opened) enzyme forms. In this case, the increase in flexibility by the mutation likely overwhelms temperature effect. DLS also indicated the formation of a more compact structure with a lower R_h upon inhibitor binding (Table 4), but only at 25 °C. KYP-2047 exerts no any compacting effect on the abhorrently "opened" (the high R_h form is 100 %) enzyme at 37 °C (Table 4 last two rows), while KYP-2047 inhibits POP completely at that condition. This could indicate that the inhibitor binds to the open form, but this is unlikely given the demonstrated domain closure that occurs upon inhibitor binding [27] and the requirement for an intact active site that is not present in the open state [27]. Alternatively, the increased R_h value could be indicative of a more flexible but still closed state for mammalian POP under these experimental conditions.

DTNB titration experiments (not shown) also demonstrated a progressive increase in the easily accessible thiol groups at increased temperature (from about 2.5 to 5 thiol groups between 25 and 37 °C), and with little difference among the various enzyme mutants. Interestingly, inhibitor-bound native POP shows a very low thiol accessibility, with only about 1.0 instantly reacting sulfhydryl group. However, mutants with reversible and weak inhibitor binding do not exhibit this behavior, suggesting that they form a less compact structure upon inhibitor binding. This decrease in flexibility and transition to a more compact structure upon ligand binding is in harmony with decreased surface loop mobility [28]. The stabilization of loop A in its closed position upon inhibitor binding can lead to a conformation restriction of the N-terminus too as these structures are coupled by the D35-K196 salt-bridge (Fig 1B). Although, crystal structures of the D149A variant and of the loop mutants would be of a great help in better understanding the mechanism of the structural dynamics, only crystals of H680A proved suitable for diffraction studies. Although the biophysical studies suggest that POP operates in a closed state, the ability of mammalian POP to adopt the open form remains unconfirmed crystallographically. The high structural homology shared with the bacterial enzyme (the closed structures superpose with an rmsd of <1 Å) would favor similar dynamics from a minimal parsimony perspective, but the relatively low amino acid sequence conservation at the domain interfaces of POPs might also favor different inter-domain stabilization and structural dynamics. The mutagenesis, enzyme kinetic and structural studies applied in this work however clearly demonstrated the highlighted importance of the flexible loops in the substrate gating thus experimentally validated the predictions of the former MD studies.

Conclusions: While the biophysical studies do not support an open resting state for mammalian POP at physiological conditions, they do not preclude it at more extreme conditions of pH, ionic strength and high protein concentration. This work unequivocally demonstrate the important contribution of the flexible loop structure (loops A, B and His) lying near the active site and domain interface to the fine-tuning of substrate entry, size selection and specificity. Manipulating this surface loop system offers a novel route for controlling catalytic activity, and represents a potential new target for inhibitor development.

Acknowledgements
We would like to thank Professor Steffen Rossner at the University of Leipzig for the human brain samples. We would also like to thank Professor Markus Forsberg at the University of Kuopio for the KYP-2047 inhibitor and to Dr. Rahfeld Jens-Ulrich (at Probiodrug) for the POP antibody. Some equipment used in this research was obtained through the Birmingham–Warwick Science City Translational Medicine: Experimental Medicine Network of Excellence project, with support from Advantage West Midlands (AWM). Crystallographic data were collected at beam line IO4 at Diamond Light Source, UK and we acknowledge the support of beam line scientist David Hall.

References

[1] L. Polgár, The prolyl oligopeptidase family, Cell Mol Life Sci, 59 (2002) 349-362.
[2] R. Mentlein, Proline residues in the maturation and degradation of peptide hormones and neuropeptides, FEBS Lett, 234 (1988) 251-256.
[3] D.F. Cunningham, B. O'Connor, Proline specific peptidases, Biochim Biophys Acta, 1343 (1997) 160-186.
[4] J.A. Garcia-Horsman, P.T. Mannisto, J.I. Venalainen, On the role of prolyl oligopeptidase in health and disease, Neuropeptides, 41 (2007) 1-24.
[5] A.J. Jalkanen, K. Savolainen, M.M. Forsberg, Inhibition of prolyl oligopeptidase by KYP-2047 fails to increase the extracellular neurotensin and substance P levels in rat striatum, Neurosci Lett, 502 107-111.
[6] T. Yoshimoto, K. Kado, F. Matsubara, N. Koriyama, H. Kaneto, D. Tsura, Specific inhibitors for prolyl endopeptidase and their anti-amnesic effect, J Pharmacobiodyn, 10 (1987) 730-735.
[7] H. Kamei, T. Ueki, Y. Obi, Y. Fukagawa, T. Oki, Protective effect of eurystatins A and B, new prolyl endopeptidase inhibitors, on scopolamine-induced amnesia in rats, Jpn J Pharmacol, 60 (1992) 377-380.
[8] K. Toide, T. Fujiwara, Y. Iwamoto, M. Shinoda, K. Okamiya, T. Kato, Effect of a novel prolyl endopeptidase inhibitor, JTP-4819, on neuropeptide metabolism in the rat brain, Naunyn Schmiedebergs Arch Pharmacol, 353 (1996) 355-362.
[9] Y. Shishido, M. Furushiro, S. Tanabe, S. Shibata, S. Hashimoto, T. Yokokura, Effects of prolyl endopeptidase inhibitors and neuropeptides on delayed neuronal death in rats, Eur J Pharmacol, 372 (1999) 135-142.
[10] C. Odaka, T. Mizuochi, T. Shirasawa, P. Morain, F. Checler, Murine T cells expressing high activity of prolyl endopeptidase are susceptible to activation-induced cell death, FEBS Lett, 512 (2002) 163-167.
[11] K.A. Puttonen, S. Lehtonen, A. Raasmaja, P.T. Mannisto, A prolyl oligopeptidase inhibitor, Z-Pro-Prolinal, inhibits glyceraldehyde-3-phosphate dehydrogenase translocation and production of reactive oxygen species in CV1-P cells exposed to 6-hydroxydopamine, Toxicol In Vitro, 20 (2006) 1446-1454.
[12] R.S. Williams, Pharmacogenetics in model systems: defining a common mechanism of action for mood stabilisers, Prog Neuropsychopharmacol Biol Psychiatry, 29 (2005) 1029-1037.
[13] I. Schulz, B. Gerhartz, A. Neubauer, A. Holloschi, U. Heiser, M. Hafner, H.U. Demuth, Modulation of inositol 1,4,5-triphosphate concentration by prolyl endopeptidase inhibition, Eur J Biochem, 269 (2002) 5813-5820.
[14] E. Di Daniel, C.P. Glover, E. Grot, M.K. Chan, T.H. Sanderson, J.H. White, C.L. Ellis, K.T. Gallagher, J. Uney, J. Thomas, P.R. Maycox, A.W. Mudge, Prolyl

oligopeptidase binds to GAP-43 and functions without its peptidase activity, Mol Cell Neurosci, 41 (2009) 373-382.
[15] I. Schulz, U. Zeitschel, T. Rudolph, D. Ruiz-Carrillo, J.U. Rahfeld, B. Gerhartz, V. Bigl, H.U. Demuth, S. Rossner, Subcellular localization suggests novel functions for prolyl endopeptidase in protein secretion, J Neurochem, 94 (2005) 970-979.
[16] M.J. Moreno-Baylach, V. Felipo, P.T. Mannisto, J.A. Garcia-Horsman, Expression and traffic of cellular prolyl oligopeptidase are regulated during cerebellar granule cell differentiation, maturation, and aging, Neuroscience, 156 (2008) 580-585.
[17] P.J. O'Reilly, M.T. Hardison, P.L. Jackson, X. Xu, R.J. Snelgrove, A. Gaggar, F.S. Galin, J.E. Blalock, Neutrophils contain prolyl endopeptidase and generate the chemotactic peptide, PGP, from collagen, J Neuroimmunol, 217 (2009) 51-54.
[18] J.M. Liu, M. Kusinski, V. Ilic, J. Bignon, N. Hajem, J. Komorowski, K. Kuzdak, H. Stepien, J. Wdzieczak-Bakala, Overexpression of the angiogenic tetrapeptide AcSDKP in human malignant tumors, Anticancer Res, 28 (2008) 2813-2817.
[19] A.R. Van Gool, R. Verkerk, D. Fekkes, S. Sleijfer, M. Bannink, W.H. Kruit, B. van der Holt, S. Scharpe, A.M. Eggermont, G. Stoter, M.W. Hengeveld, Plasma activity of prolyl endopeptidase in relation to psychopathology during immunotherapy with IFN-alpha in patients with renal cell carcinoma, J Interferon Cytokine Res, 28 (2008) 283-286.
[20] V. Fülöp, Z. Böcskei, L. Polgár, Prolyl oligopeptidase: an unusual beta-propeller domain regulates proteolysis, Cell, 94 (1998) 161-170.
[21] L. Polgár, Prolyl endopeptidase catalysis. A physical rather than a chemical step is rate-limiting, Biochem J, 283 (1992) 647-648.
[22] V. Fülöp, Z. Szeltner, L. Polgár, Catalysis of serine oligopeptidases is controlled by a gating filter mechanism, EMBO Rep, 1 (2000) 277-281.
[23] T. Juhász, Z. Szeltner, V. Fülöp, L. Polgár, Unclosed beta-propellers display stable structures: implications for substrate access to the active site of prolyl oligopeptidase, J Mol Biol, 346 (2005) 907-917.
[24] Z. Szeltner, D. Rea, T. Juhász, V. Renner, V. Fülöp, L. Polgár, Concerted structural changes in the peptidase and the propeller domains of prolyl oligopeptidase are required for substrate binding, J Mol Biol, 340 (2004) 627-637.
[25] M. Fuxreiter, C. Magyar, T. Juhász, Z. Szeltner, L. Polgár, I. Simon, Flexibility of prolyl oligopeptidase: molecular dynamics and molecular framework analysis of the potential substrate pathways, Proteins, 60 (2005) 504-512.
[26] L. Shan, Mathews, II, C. Khosla, Structural and mechanistic analysis of two prolyl endopeptidases: role of interdomain dynamics in catalysis and specificity, Proc Natl Acad Sci U S A, 102 (2005) 3599-3604.
[27] M. Li, C. Chen, D.R. Davies, T.K. Chiu, Induced-fit mechanism for prolyl endopeptidase, J Biol Chem, 285 21487-21495.
[28] K. Kaszuba, T. Róg, R. Danne, P. Canning, V. Fülöp, T. Juhász, Z. Szeltner, J.F. St Pierre, A. García-Horsman, P.T. Männistö, M. Karttunen, J. Hokkanen, A. Bunker, Molecular dynamics, crystallography and mutagenesis studies on the substrate gating mechanism of prolyl oligopeptidase, Biochimie, 94 1398-1411.
[29] Z. Szeltner, V. Renner, L. Polgár, Substrate- and pH-dependent contribution of oxyanion binding site to the catalysis of prolyl oligopeptidase, a paradigm of the serine oligopeptidase family, Protein Sci, 9 (2000) 353-360.
[30] R.J. Leatherbarrow, Grafit, Version 5.0, Erithacus Software Ltd. Horley, U.K., (2001).
[31] Cornish-Bowden, Fundamentals of Enzyme Kinetics, Portland Press Ltd, London, United Kingdom, 1995.

[32] P.K. Glassoe, F.A. and Long, Use of glass electrodes to measure acidities in deuterium oxide., J. Phys. Chem., 64 (1960) 188-190.
[33] R.K. Bryan, Solving oversampled data problems by maximum entropy. In Maximum Entropy and Bayesian Methods, Kluwer Academic Publishers (1990), The Netherlands
[34] W. Kabsch, Automatic processing of rotation diffraction data from crystals of initially unknown symmetry and cell constants, J. Appl. Cryst., 26 (1993) 795-800.
[35] C.C. Project, The CCP4 suite: programs for protein crystallography, in, vol. D50, Acta Crystallography, 1994, pp. 760-763.
[36] G.N. Murshudov, A.A. Vagin, A. Lebedev, K.S. Wilson, E.J. Dodson, Efficient anisotropic refinement of macromolecular structures using FFT, Acta Crystallogr D Biol Crystallogr, 55 (1999) 247-255.
[37] T.A. Jones, J.Y. Zou, S.W. Cowan, M. Kjeldgaard, Improved methods for building protein models in electron density maps and the location of errors in these models, Acta Crystallogr A, 47 (Pt 2) (1991) 110-119.
[38] A. Perrakis, R. Morris, V.S. Lamzin, Automated protein model building combined with iterative structure refinement, Nat Struct Biol, 6 (1999) 458-463.
[39] L. Polgár, Effects of ionic strength on the catalysis and stability of prolyl oligopeptidase, Biochem J, 312 (1995) 267-271.
[40] Z. Szeltner, V. Renner, L. Polgár, The noncatalytic beta-propeller domain of prolyl oligopeptidase enhances the catalytic capability of the peptidase domain, J Biol Chem, 275 (2000) 15000-15005.
[41] Z. Szeltner, M. Morawski, T. Juhász, I. Szamosi, K. Liliom, V. Csizmók, F. Tölgyesi, L. Polgár, GAP43 shows partial co-localisation but no strong physical interaction with prolyl oligopeptidase, Biochim Biophys Acta, 1804 (2010) 2162-2176.
[42] Z. Szeltner, D. Rea, V. Renner, L. Juliano, V. Fülöp, L. Polgár, Electrostatic environment at the active site of prolyl oligopeptidase is highly influential during substrate binding, J Biol Chem, 278 (2003) 48786-48793.
[43] Z. Szeltner, D. Rea, T. Juhász, V. Renner, Z. Mucsi, G. Orosz, V. Fülöp, L. Polgár, Substrate-dependent competency of the catalytic triad of prolyl oligopeptidase, J Biol Chem, 277 (2002) 44597-44605.
[44] W.M. Nolte, D.M. Tagore, W.S. Lane, A. Saghatelian, Peptidomics of prolyl endopeptidase in the central nervous system, Biochemistry, 48 (2009) 11971-11981.
[45] L. Polgár, A. Patthy, Cleavage of the Lys196-Ser197 bond of prolyl oligopeptidase: enhanced catalytic activity for one of the two active enzyme forms, Biochemistry, 31 (1992) 10769-10773.
[46] T. Tarrago, J. Martin-Benito, E. Sabido, B. Claasen, S. Madurga, M. Gairi, J.M. Valpuesta, E. Giralt, A new side opening on prolyl oligopeptidase revealed by electron microscopy, FEBS Lett, 583 (2009) 3344-3348.
[47] V. Harmat, K. Domokos, D.K. Menyhárd, A. Palló, Z. Szeltner, I. Szamosi, T. Beke-Somfai, G. Náray-Szabó, L. Polgár, Structure and catalysis of acylaminoacyl peptidase: closed and open subunits of a dimer oligopeptidase, J Biol Chem, 286 (2011) 1987-1998.
[48] N. Kichik, T. Tarrago, B. Claasen, M. Gairi, O. Millet, E. Giralt, (15) N Relaxation NMR Studies of Prolyl Oligopeptidase, an 80 kDa Enzyme, Reveal a Pre-existing Equilibrium between Different Conformational States, Chembiochem, (2011).
[49] P. Salers, Evidence for the presence of prolyl oligopeptidase and its endogenous inhibitor in neonatal rat pancreatic beta-cells, Regul Pept, 50 (1994) 235-245.
[50] J. Tenorio-Laranga, F. Coret-Ferrer, B. Casanova-Estruch, M. Burgal, J.A. Garcia-Horsman, Prolyl oligopeptidase is inhibited in relapsing-remitting multiple sclerosis, J Neuroinflammation, 7 23.

[51] D. Rea, V. Fülöp, Prolyl oligopeptidase structure and dynamics, CNS Neurol Disord Drug Targets, 10 306-310.
[52] R.J. Read, Improved Fourier coefficients for maps using phases from partial structures with errors, Acta Crystallography, A42 (1986) 140-149.
[53] W.L. DeLano, The PyMOL User s Manual, DeLano Scientific, Palo Alto (2002) CA.
[54] A.T. Brunger, Free R value: a novel statistical quantity for assessing the accuracy of crystal structures, Nature, 355 (1992) 472-475.
[55] D.W. Cruickshank, Remarks about protein structure precision, Acta Crystallogr D Biol Crystallogr, 55 (1999) 583-601.

Figure captions

Fig. 1. Schematic representation of the structure of POP. (A) The overall structure of POP. (B) Part of POP, comprising the flexible loop structure. Loop A (res. 189-209) of the propeller, loop B (res. 577-608) of the catalytic domain and the loops holding D641, His680 and Cys255 are shown in black. The part of the N-terminus holding D35 are also shown as well as the loop that holds D149 (in white and signed with D). The mutated residues, the catalytic amino acids, the amino acids forming the K196-D35 salt-bridge and some other catalytically important residues, W595, R643, H593 and are highlighted and shown in wireframe representation. The inhibitor, Z-Pro-prolinal forming a hemiacetal to S554 is shown in black. The figures were made by Swiss PDB Viewer (4.04) and rendered with POV-Ray 3.6.

Fig. 2. Structural studies of the wild-type and the loop A^- POP. **(**A) CD spectra in the near-UV region. Wild-type (continuous line) and loop A^- POP (dotted line). (B) DSC thermograms show two-transition thermal denaturation for both the wild-type (closed circle) and the variant enzyme (open circle).

Fig. 3. pH dependence of the specificity rate constant (k_{cat}/K_m) of POP variants with substrate Z-Gly-Pro-BNA, measured in standard buffer. (A) Wild-type enzyme (downward triangle) and T204A (open circle). (B) T202C variant (open square) and T202C variant at 300 mM NaCl (black line). (C) T202C/T590C (upward triangle) and D149A (x). (D) Loop A^- (open circle) and loop A^- at plus 300 mM NaCl (filled circle) concentration. The fitted parameters are found in Table 1. Inserts in Fig. A, B and D show the pH dependent kinetic deuterium isotope effects.

Fig. 4. Specificity and ionic strength sensitivity of the POP variants. The rate constants were measured in standard buffer at discrete pH values (pH 7.0 and 8.0) and at two ionic strengths (without added NaCl and at plus 300 mM NaCl). Substrate sequences are found in the Materials and methods section. The asterisk indicates substrate inhibition at the applied substrate concentration. The transparent bars show the values at low ionic strength. (A) and (A') Loop A^- variant at pH 7.0 and at pH 8.0, respectively. (B) T202C/T590C variant at pH 7.0. (C) Wild-type POP at pH 8.0. (E) and (E) Loop A^- POP at pH 7.0 and at pH 8.0, respectively.

Fig. 5. Inhibition and binding of wild-type POP and the loop A^- variant with KYP-2047. **(**A) The inhibitor binds very strongly and irreversibly (K_i=0.13 ± 0.006 nM) to the wild-type enzyme (filled circle). (Insert of A) Inhibitor binding causes a change in the mobility of the main form of POP, (labeled I) to a more compact form. (B) KYP-2047 binds 7700-fold less

efficiently (K_i=1,015 ± 117 nM) and reversibly to the loop A^- variant (open circle). (Insert of B) No change in the relative abundance or mobility of the forms are observed upon incubation of the loop A^- variant with inhibitor. The measurements were carried out at 25 °C in standard buffer at pH 8.0. Native PAGE was carried out with the method of Laemmli (1970).

Fig. 6. Interaction between a heptadecapeptide substrate (Abz-Gly-Phe-Ser-Pro-Phe-Arg-Ser-Ser-Arg-Ile-Gly-Glu-Ile-Lys-Glu-Glu-Gln-EDDnp) and POP. (A) and (B) Substrate inhibition of POP. The measurement were carried out in standard buffer and at pH 8.0. Both the specificity rate constant (k_{cat}/K_m) (A) and the initial rate (B) increased exponentially as the substrate was reduced up to the sensitivity limit of the instrument. The approximate K_i of the self-inhibition is 250 ± 20 nM. (C) DSC scans of S554A POP in the presence of substrates. POP without substrate (black line), with the heptapeptide as control at 26 µM (gray curve) and with the heptadecapeptide substrates at 26 µM (open circles). (D) POP with various concentrations (0.0, 3.0, 10.0 and 26 µM) of the heptadecapeptide substrate (colored from black to light gray).

Fig. 7. DSC scans of POP variants. (A) Wild-type POP (open circle), HIS-tagged (dotted line) and D149A (continuous black line) POP variants display a dual-transition thermal denaturation, but with a significantly different shape of the transition curve. Inhibitor binding to wild-type POP (filled circle) abolishes the first transition and causes an increased T_m in the second transition. (B) Inhibitor binding to the loop A^- variant (dotted black curve), and to the T202C/T590C (continuous black curve) variants. The first transitions merge partially (dotted grey curve) or fully (continuous grey curve), into the second transition respectively. (C) Step-heating DSC scans with sequential heating and re-cooling cycles from: 25°C-41.7 °C (2) and back to 25 °C, from 25°C-48.5 °C (3) and back to 25 °C, from 25°C-51.6 °C (4) and back to 25 °C, and from 25°C-55.4 °C (5) and back to 25 °C. A scan for the whole temperature interval from 25-70 °C was also executed (1). Insert of (C) Native PAGE of POP after heated to 45 °C (I), 47.5 °C (II), 50 °C (III), and 60°C (IV). Samples were heated in 20 mM phosphate buffer at pH 8.0 and native PAGE was carried out with the method of Laemmli (1970). (D) DSC profile of the oxidized (disulfide bridged) T202C/T590C variant with (continuous grey curve) and without (continuous black curve) KYP-2047. Formation of the chemical cross-link between loop A and loop B prevents the appearance of the first transition. Inhibitor cannot bind and cannot modify the melting curve significantly.

Fig. 8. Native PAGE with recombinant and native POP. **(**A) Recombinant POP in complete Laemmli native gel containing a stacking gel. Three POP forms can be observed; the most compact form (1), a less mobile and likely open form (2), and a likely oligomeric form (3). (B) Recombinant POP in native gel without stacking gel. Only form (1) is present. (C) Native immunoblot detecting the two main forms for the recombinant, but only the most compact form for the endogenous POP. The * signs no POP, but an artifact band caused by the hemoglobin content in the samples.

Fig. 9. Dynamic light-scattering profiles of POP at different experimental conditions (pH and ionic strength) at 25 °C. The R_h values (seen in Table 4) describe the hydrodynamic volume(s) of the population(s) of POP. Where the polydispersity index (see in the insert) was higher than 0.04, curves were considered to represent more than one component. The parameters for the curves not presented in Fig. 9. are found in Table 4.

Fig. 10. Structural comparison of the H680A variant and native POP. The native structure and the H680A structure are shown in wireframe and stick representation, respectively. Important hydrogen bonds are shown as dotted lines. The SIGMAA [52] weighted $2mF_O$-ΔF_C electron density using phases from the final H680A model is contoured at the 1.5 σ level, where σ represents the RMS electron density for the unit cell. Contours more than 1.5 Å from any of the displayed atoms have been removed for clarity. Thin lines indicate hydrogen bonds. Drawn with PyMOL [53].

Table 1. Kinetic parameters for the reactions of POP variants with substrate Z-Gly-Pro-BNA

Variant	**pK_1**	**pK_2**	**k(limit)$_1$ (mM^{-1} s^{-1})**	**k(limit)$_2$ (mM^{-1} s^{-1})**	**pK_3**
Wild-type POP	4.89	7.07	1108	4664	9.17
T202C	6.09	7.26	9932	1524	8.83
T202C + 300 mM salt	6.15	7.48	13271		
[a]Trypsin-cleaved POP	5.96	7.56	7500	1453	8.97
T202C/T590C POP	6.55	6,82	194	39.0	8.14
[a]Loop A^- POP	5.86	7.36	0.34	0.16	8.92
Loop A^- POP + 300 mM salt	5.80	8.68	0.34		
D149A	5.92	7.01	47.3	10.1	9.90

[a]From [28]

Table 2. Change in the preference of POP for the short Z-Gly-Pro-BNA over the bulkier Abz-Gly-Phe- Gly-Pro-Phe-Gly-Phe(NO_2)-Ala substrate upon oxidation of POP variants.

Variant	**At the beginning of oxidation** [a]	**At the end of the oxidation by air** [a]	**At the end of the oxidation by GSSG/GSH** [a]
Wild-type POP	1.30 -1.83	1.46	1.12
C255S	1.07	0.93	0.82
T202C/T590C	6.30	10.3	24.3

[a]The ratio of the specificity rate constants of the short vs. long substrates.

Table 3. Kinetic parameters of POP and its variants.

Variant	k_{cat} [b] (sec^{-1})	K_m [b] (μM)	K_{cat}/K_m [a] ($M^{-1}s^{-1}$)	K_i [a] (nM)
Wild-type POP	0.97 ± 0.16	0.81 ± 0.13	~4,400,000	0.132 ± 0.006
T202C/T590C POP	1.31 ± 0.22	9.21 ± 0.85	~60,000	nd.
Loop A^- POP	0.076 ±0.011	162 ± 22	~200	1,015 ± 117

[a]Measured with Z-Gly-Pro-BNA at first-order condition at pH 8.0.
[b]Measured with the highly water soluble Abz-Gly-Phe-Arg-Pro-Phe(NO_2)-Arg-Ala at pH 8.0 using initial velocity or progress curve studies.

Table 4. Size distribution of POP and its variants at various conditions

Conditions	**Peak 1** R_h (nm)	**Peak 2** R_h (nm)	**Peak 1** R_h RMSD (nm)	**Peak 2** R_h RMSD (nm)	**Peak 1** Area %	**Peak 2** Area %
Wild-type (pH 6.5, no salt) 25 °C	-	3.44	-	0.004	0	100
Wild-type (pH 6.5, no salt + KYP-2047) 25 °C	3.00	3.45	0.020	0.100	75	25
Wild-type (pH 6.5 + 300 mM NaCl) 25 °C	3.03	3.56	0.082	0.220	56	44
Wild-type (pH 8.0, no salt) 25 °C	3.10	3.77	0.050	0.140	57	43
Wild-type (pH 8.0, no salt + KYP-2047) 25 °C	3.24	-	0.017	-	100	0
Wild-type (pH 8.0 + 300 mM NaCl) 25 °C	-	3.60	-	0.170	0	100
D149A (pH 8.0 + 300 mM NaCl) 25 °C	3.57	4.22	0.033	0.290	56	44
D149A (pH 7.4 + 150 mM NaCl) 25 °C	3,47	4.07	0.031	0.062	55	45
D149A (pH 7.4 + 150 mM NaCl) 37 °C	3.28	4.04	0.045	0.059	51	49
Loop A^- (pH 7.4 + 150 mM NaCl) 25 °C	2.52	3.70	0.056	0.011	9	91
T202C/T590C (pH 7.4 + 150 mM NaCl) 25 °C	3.00	3.84	0.032	0.059	58	42
Wild-type (pH 7.4 + 150 mM NaCl) 25 °C	3.13	3.68	0.035	0.068	56	44
Wild-type (pH 7.4 + 150 mM NaCl) 37 °C	-	3.60	-	0.003	0	100
Wild-type (pH 7.4 + 150 mM NaCl) 37 °C + KYP-2047	-	3.68	-	0.028	0	100

Table 5. Summary of crystallographic data collection and refinement statistics

Data collection	
Synchrotron radiation, detector and	Diamond, IO4, ADSC Q315r CCD
wavelength (Å)	0.9795
Unit cell (Å)	a= 71.08, b= 99.08, c= 110.06
Space group	$P2_12_12_1$
Resolution (Å)	50-1.6 (1.69-1.6)
Observations	500,458
Unique reflections	101,085
I/σ(I)	11.1 (2.0)
R_{sym}[a]	0.091 (0.781)
Completeness (%)	98.6 (99.3)
Refinement	
Non-hydrogen atoms	6,444 (including 9 glycerols & 765 waters)
R_{cryst}[b]	0.163 (0.303)
Reflections used	96,969 (7,118)
R_{free}[c]	0.196 (0.318)
Reflections used	4116 (315)
R_{cryst} (all data)[b]	0.164
Average temperature factor (Å^2)	17.3
Rmsds from ideal values	
Bonds (Å)	0.015
Angles (^{o})	1.5
DPI coordinate error (Å)	0.08

Numbers in parentheses refer to values in the highest resolution shell.

[a] $R_{sym} = \Sigma_j\Sigma_h|I_{h,j} - \langle I_h\rangle|/\Sigma_j\Sigma_h\langle I_h\rangle$ where $I_{h,j}$ is the jth observation of reflection h, and $\langle I_h\rangle$ is the mean intensity of that reflection

[b] $R_{cryst} = \Sigma||F_{obs}|-|F_{calc}||/\Sigma|F_{obs}|$ where F_{obs} and F_{calc} are the observed and calculated structure factor amplitudes, respectively

[c] R_{free} is equivalent to R_{cryst} for a 4% subset of reflections not used in the refinement [54]

[d] DPI refers to the diffraction component precision index [55]

Fig. 1.

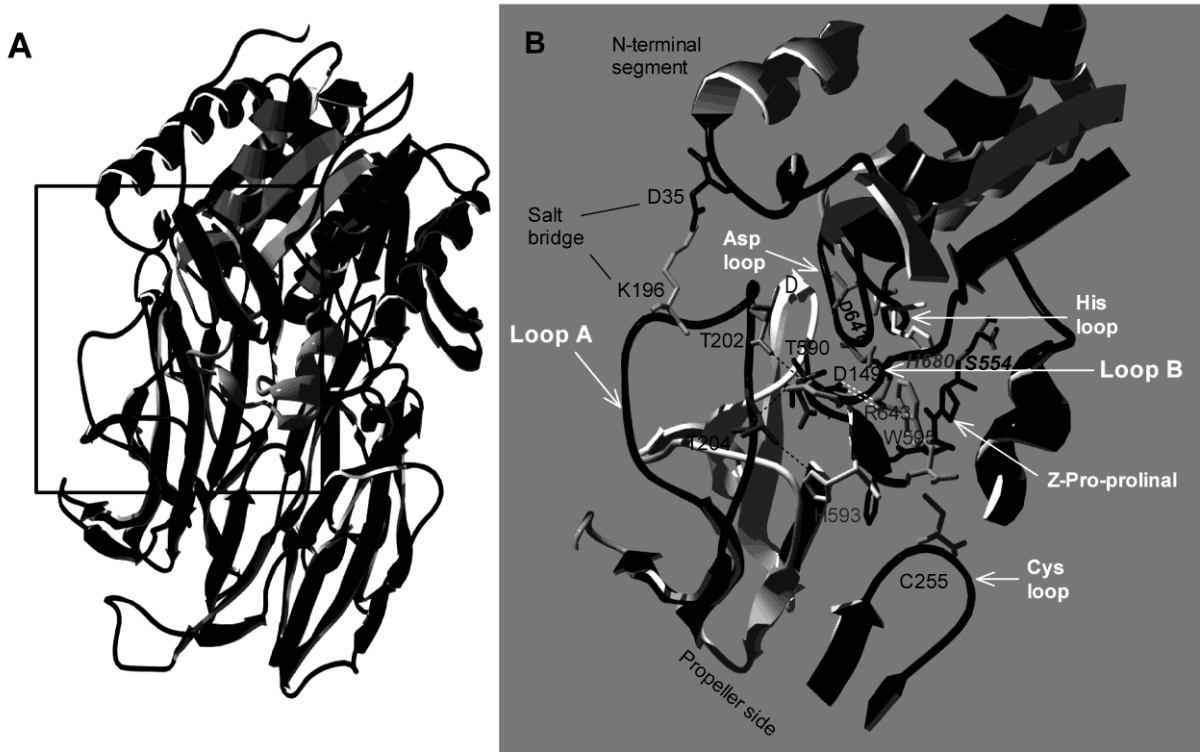
A
B
N-terminal segment
Salt bridge
D35
K196
Asp loop
D
D64
His loop
Loop A
T202
T590
D149
H680
S554
Loop B
R643
W596
T204
Z-Pro-prolinal
H593
C255
Cys loop
Propeller side

Fig. 2.

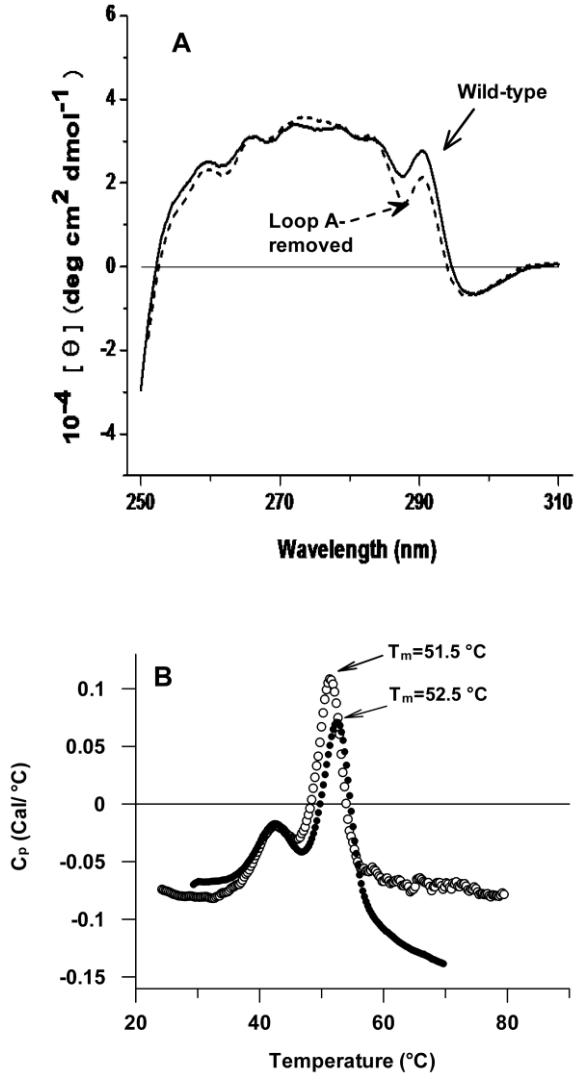
A
Wild-type
Loop A-removed
10^{-4} [θ] (deg cm^2 dmol^{-1})
Wavelength (nm)
B
T_m=51.5 °C
T_m=52.5 °C
C_P (Cal/ °C)
Temperature (°C)

Fig. 3.

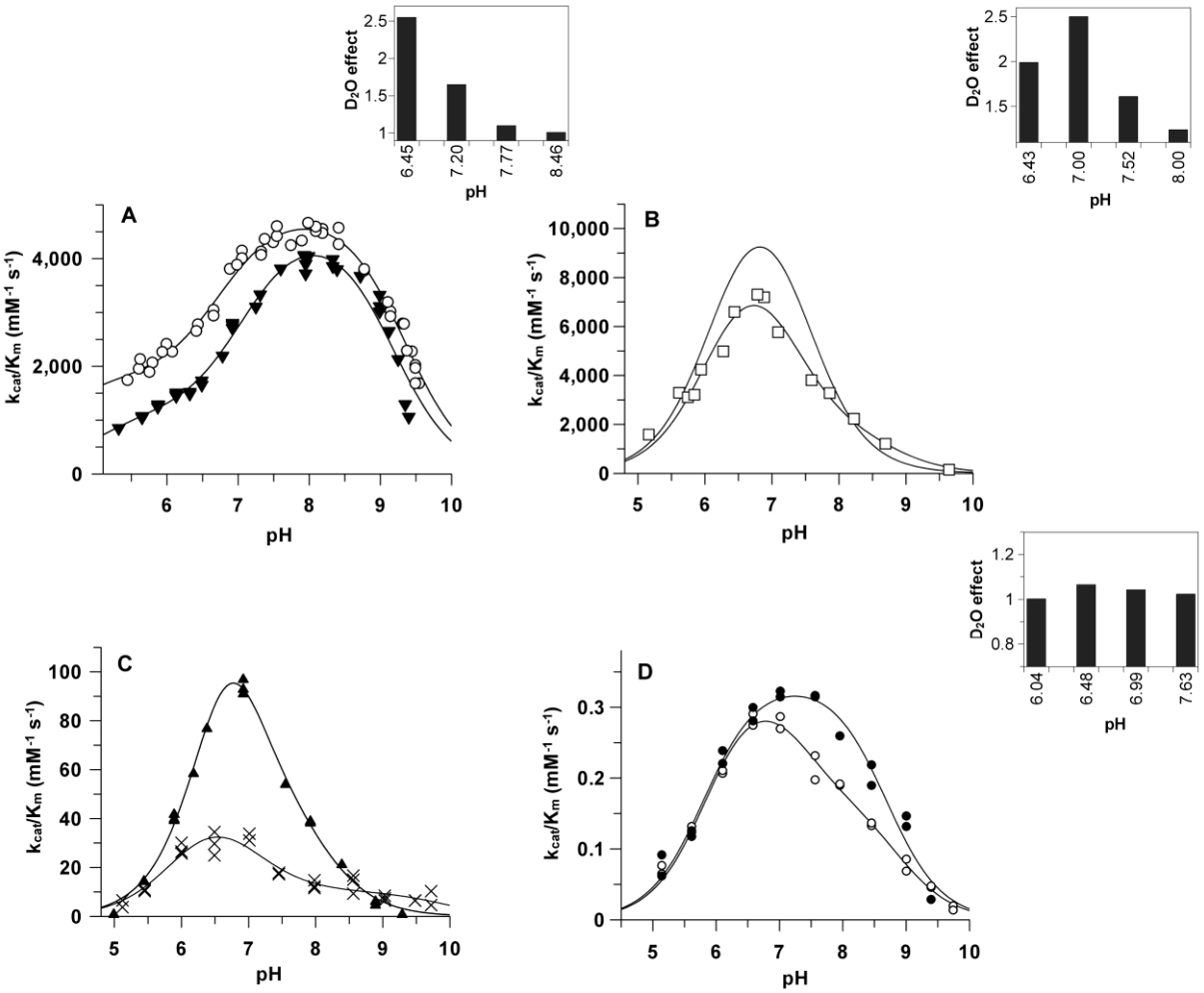
A
B
C
D
k_{cat}/K_m (mM^{-1} s^{-1})
pH
D_2O effect
6.45
7.20
7.77
8.46
6.43
7.00
7.52
8.00
6.04
6.48
6.99
7.63

Fig. 4.

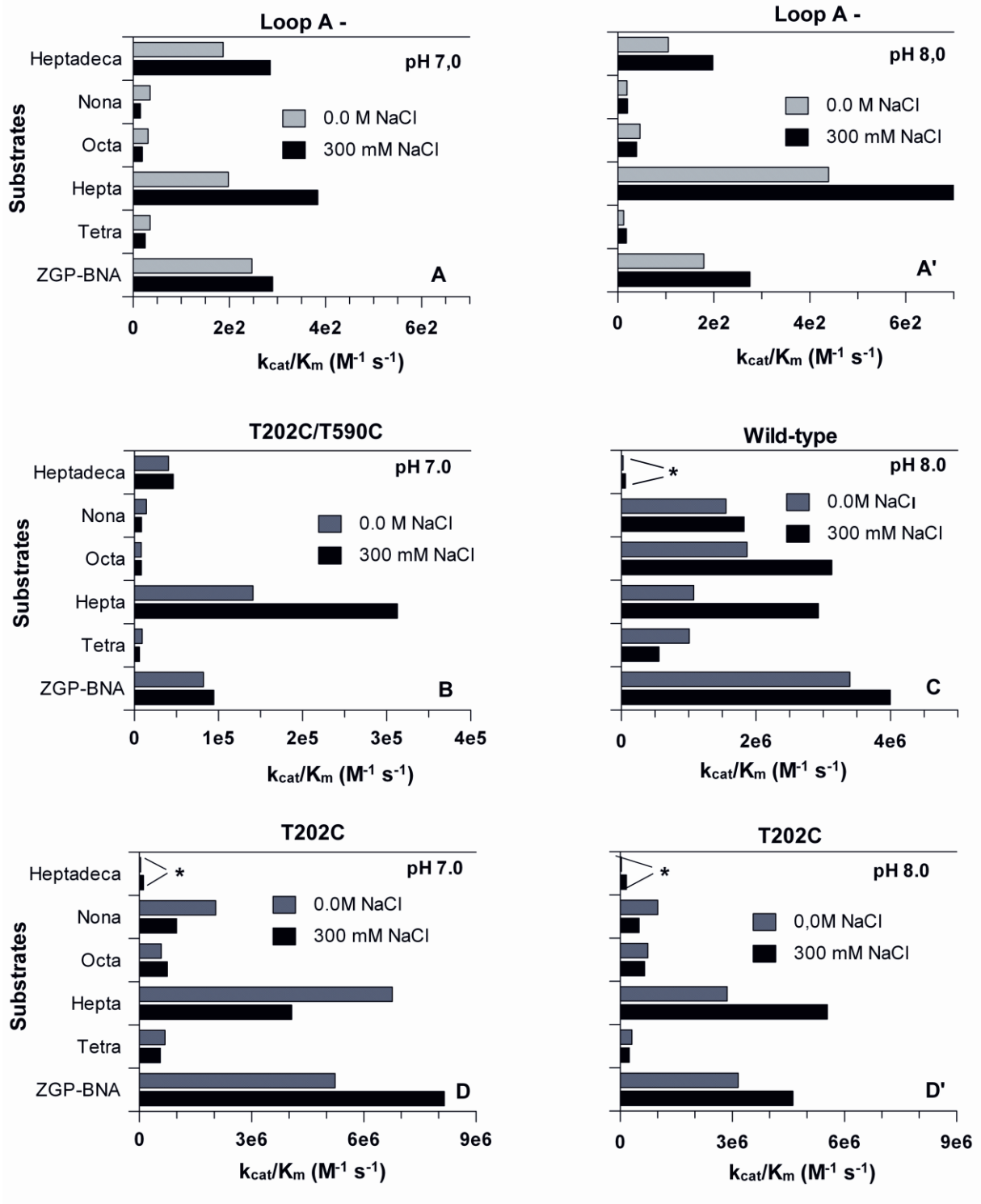
Loop A -
pH 7,0
0.0 M NaCl
300 mM NaCl
Substrates
Heptadeca
Nona
Octa
Hepta
Tetra
ZGP-BNA
A
0
2e2
4e2
6e2
kcat/Km (M-1 s-1)
Loop A -
pH 8,0
0.0 M NaCl
300 mM NaCl
A'
0
2e2
4e2
6e2
kcat/Km (M-1 s-1)
T202C/T590C
pH 7.0
0.0 M NaCl
300 mM NaCl
Substrates
Heptadeca
Nona
Octa
Hepta
Tetra
ZGP-BNA
B
0
1e5
2e5
3e5
4e5
kcat/Km (M-1 s-1)
Wild-type
pH 8.0
*
0.0M NaCl
300 mM NaCl
C
0
2e6
4e6
kcat/Km (M-1 s-1)
T202C
pH 7.0
*
0.0M NaCl
300 mM NaCl
Substrates
Heptadeca
Nona
Octa
Hepta
Tetra
ZGP-BNA
D
0
3e6
6e6
9e6
kcat/Km (M-1 s-1)
T202C
pH 8.0
*
0,0M NaCl
300 mM NaCl
D'
0
3e6
6e6
9e6
kcat/Km (M-1 s-1)

Fig. 5.

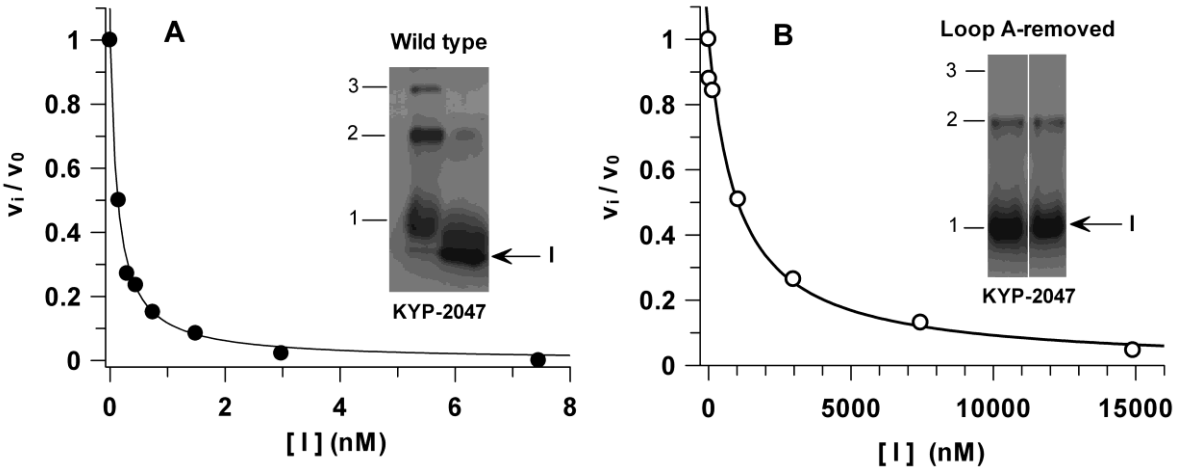
A
Wild type
3
2
1
I
KYP-2047
v_i / v_0
1
0.8
0.6
0.4
0.2
0
0
2
4
6
8
[I] (nM)
B
Loop A-removed
3
2
1
I
KYP-2047
v_i / v_0
1
0.8
0.6
0.4
0.2
0
0
5000
10000
15000
[I] (nM)

Fig. 6.

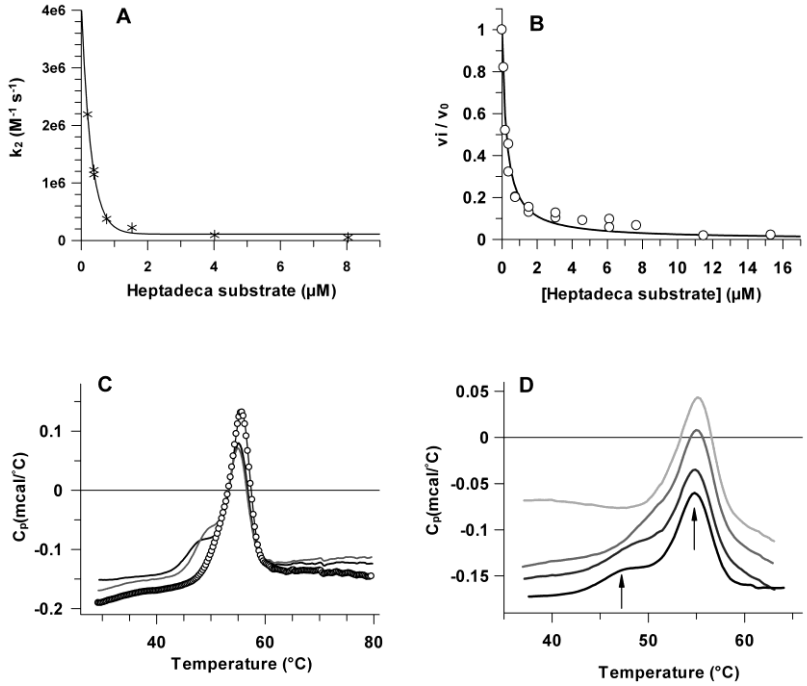
A
B
C
D
k2 (M-1 s-1)
Heptadeca substrate (μM)
vi / v0
[Heptadeca substrate] (μM)
Cp(mcal/°C)
Temperature (°C)
Cp(mcal/°C)
Temperature (°C)

Fig. 7.

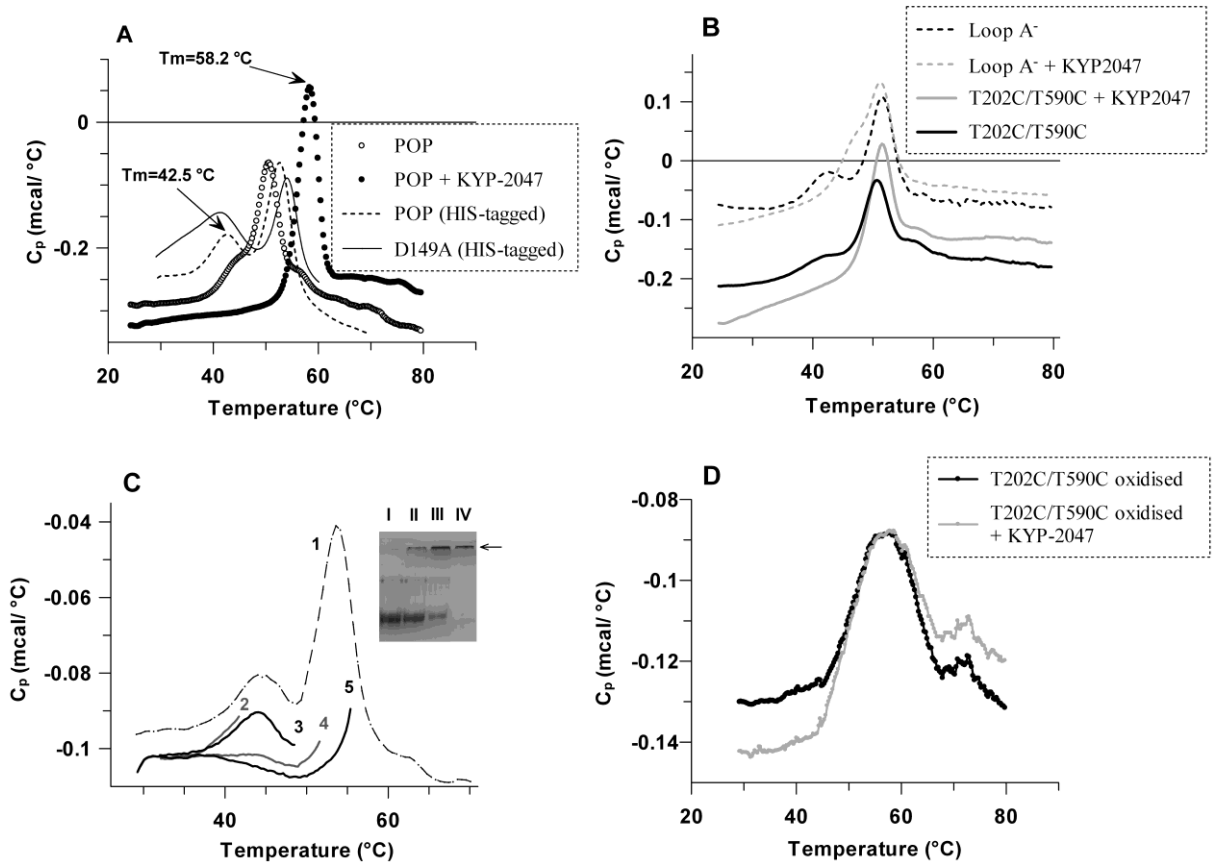
A
Tm=58.2 °C
Tm=42.5 °C
POP
POP + KYP-2047
POP (HIS-tagged)
D149A (HIS-tagged)
Cp (mcal/ °C)
Temperature (°C)
B
Loop A-
Loop A- + KYP2047
T202C/T590C + KYP2047
T202C/T590C
C
I II III IV
1
2
3
4
5
D
T202C/T590C oxidised
T202C/T590C oxidised + KYP-2047

Fig. 8.

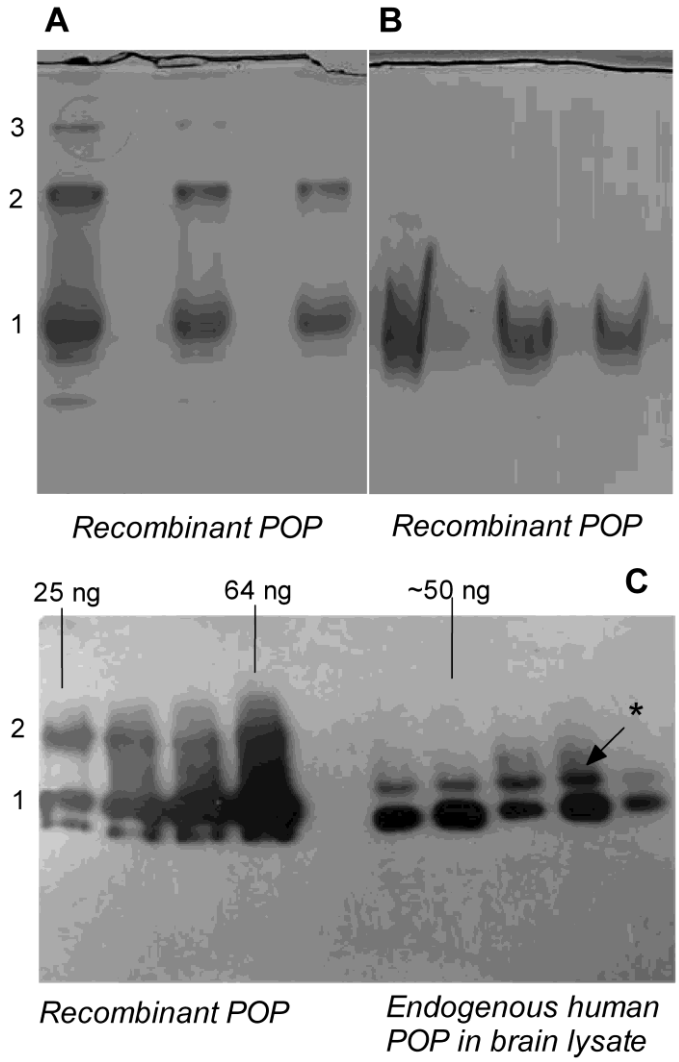
A
B
3
2
1
Recombinant POP
Recombinant POP
25 ng
64 ng
~50 ng
C
2
1
*
Recombinant POP
Endogenous human
POP in brain lysate

Fig. 9.

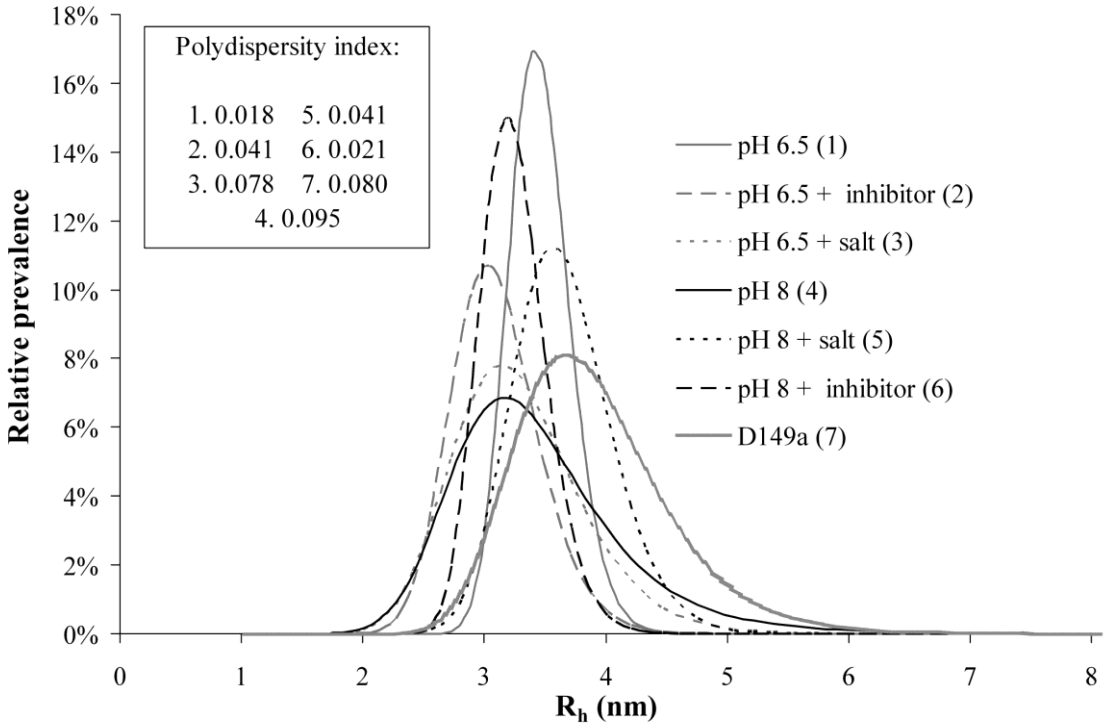
Polydispersity index:
1. 0.018
2. 0.041
3. 0.078
4. 0.095
5. 0.041
6. 0.021
7. 0.080
pH 6.5 (1)
pH 6.5 + inhibitor (2)
pH 6.5 + salt (3)
pH 8 (4)
pH 8 + salt (5)
pH 8 + inhibitor (6)
D149a (7)
Relative prevalence
18%
16%
14%
12%
10%
8%
6%
4%
2%
0%
0
1
2
3
4
5
6
7
8
Rh (nm)

Fig. 10.

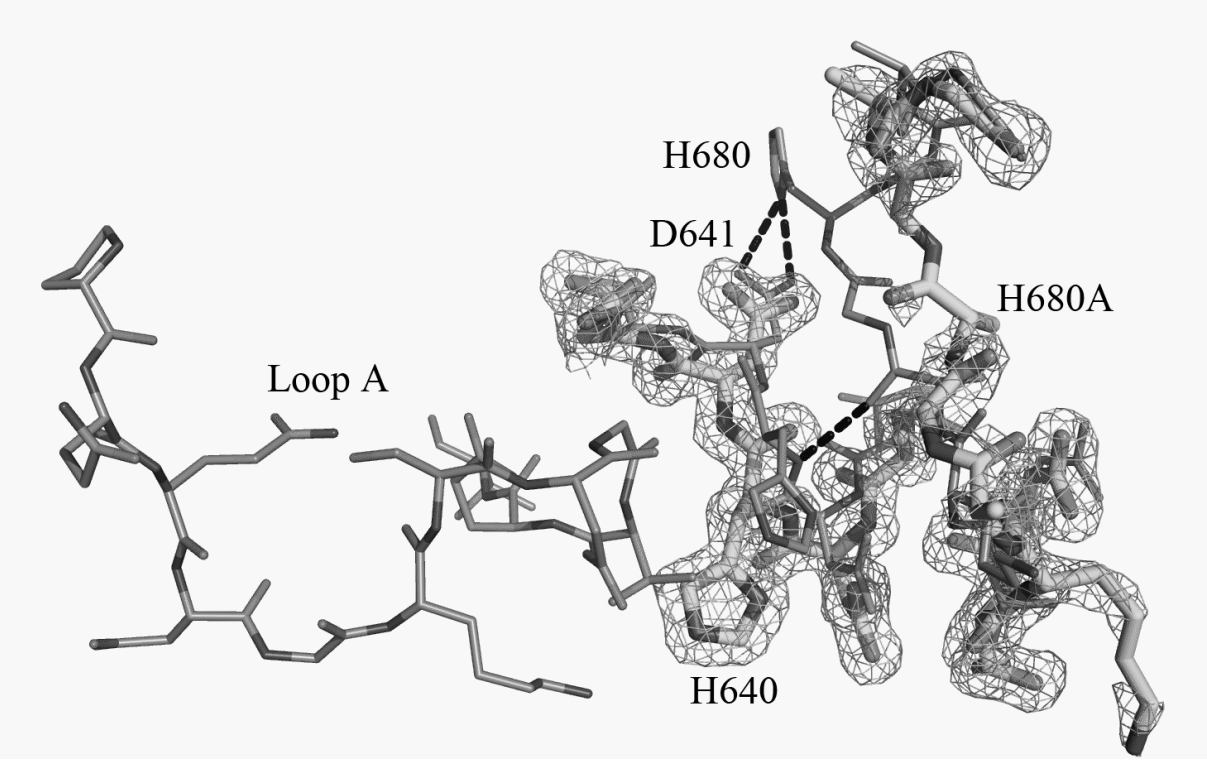

Highlights

- **Prolyl oligopeptidase (POP) has emerged as a drug target for neurological diseases.**
- **Mutations in the flexible loops at the entrance of the active site of POP greatly influence the catalytic power, ligand-binding capacity and the specificity of POP.**
- **The interaction between loop A, loop B and the N-terminus of POP is crucial in substrate gating and fine-tunes potential inter-domain fluctuations during catalysis.**
- **The flexible loop system of POP represents a potential new target for inhibitor development.**